VIRTUAL MILLING

By

Isabelle Bélanger

B.Eng. Ecole Polytechnique de Montréal, Canada, 1996

A THESIS SUBMITTED IN PARTIAL FULFILLMENT OF
THE REQUIREMENTS FOR THE DEGREE OF

MASTER OF APPLIED SCIENCE

in

The Faculty of Graduate Studies

Department of Mechanical Engineering

We accept this thesis as conforming
to the required standard

THE UNIVERSITY OF BRITISH COLUMBIA

April 2004

Library Authorization

In presenting this thesis in partial fulfillment of the requirements for an advanced degree at the University of British Columbia, I agree that the Library shall make it freely available for reference and study. I further agree that permission for extensive copying of this thesis for scholarly purposes may be granted by the head of my department or by his or her representatives. It is understood that copying or publication of this thesis for financial gain shall not be allowed without my written permission.

ISABELLE BÉLANGER — 19/04/2004

Name of Author *(please print)* — Date (dd/mm/yyyy)

Title of Thesis: VIRTUAL MILLING

Degree: MASTER OF APPLIED SCIENCE Year: 2004

Department of MECHANICAL ENGINEERING

The University of British Columbia
Vancouver, BC Canada

Abstract

Milling is used to manufacture a wide variety of metal parts, from simple to complex geometries, in small or large volumes. The requirements for these parts usually necessitate that the milling operation is accurate, but also the production rate must be as high as possible. These two requirements, which appear conflicting as first, are met if the milling operation is well planned. While NC programming is still based in many industries on past experience and practical knowledge, research in the areas of cutting mechanics, modelling and simulation are gradually changing the manufacturing practices.

This thesis investigates Virtual Milling, which is the integration of milling simulation and CAD/CAM capabilities. Available milling simulation systems can simulate the process for one set of cutting conditions. The objective with Virtual Milling is to not only simulate the milling operation for the whole NC program, but also to integrate features such as feedrate scheduling.

A milling simulation for the whole part was developed based on the analytical closed-loop milling model presented by Spence[36]. The input to the simulation is the cutter-workpiece intersections along the tool path. The simulation results include force, torque and power, and deflection along the tool path.

The second part of this thesis is the implementation of a Virtual Milling framework. The first step is the selection of cutting conditions which is done during the NC programming. CAD/CAM software do not provide tools to select appropriate cutting conditions, therefore we established the requirements for such a tool using stability lobe theory. An interface was implemented in a commercial CAD/CAM software to demonstrate this. The milling simulation is then used to identify critical locations along the tool path, and it is also used to perform feedrate scheduling. Two off-line approaches for feedrate scheduling were implemented, constraint-based feedrate scheduling and off-line adaptive force control, and evaluated to see if their use would lead to improved

machining accuracy, better control of cutting forces, and improved machining time. Cutting tests were conducted and these approaches were also compared to an existing online adaptive force control.

Table of Contents

List of Figures

Acknowledgements

First, I would like to thank Dr Yusuf Altintas for his supervision, encouragement and guidance throughout this project. I would also like to thank the members of the examining committee, Dr Sassani and Dr Yip-Hoi, for their feedback on the thesis. Also, my colleagues from the Manufacturing Automation Laboratory (Kaan, Simon, Jochem, Yuzhong, Eva, Xuemei, Chi-Ho, Dima, and many others) for their support and for sharing with them the experience of graduate studies. I would like to thank specifically Fuat Atabey, Merhdad Nevis, Simon Park and Dr Xuemei Huang for their precious help during the project.

Je tiens également à remercier ma famille (Lucide, Laurent, Marc-André et sa conjointe Catherine) pour leur support et encouragement au cours des années, mes amis à Montréal et Vancouver, et finalement, un remerciement spécial à Florian pour son support au cours des derniers mois de rédaction.

Nomenclature

a_{lim}	chatter-free axial depth of cut [mm]
f_a	actual feedrate delivered [mm/min]
f_c	command feedrate [mm/min]
h	uncut chip thickness [mm]
h_{max}	maximum chip load [mm]
i	surface number
j	tooth number : 0 to N-1
k_t	static stiffness [N/mm]
k	element k for deflection model
l, L	tool length [mm]
n	spindle speed [rad/s] or [rpm]
s_t	feedrate [mm/tooth]
$s_{t,chip}$	adjusted feedrate for chip load constraint [mm/tooth]
$s_{t,def}$	adjusted feedrate for deflection constraint [mm/tooth]
$s_{t,force}$	adjusted feedrate for force constraint [mm/tooth]
$s_{t,opt}$	maximum allowable feedrate [mm/tooth]
$s_{t,torque}$	adjusted feedrate for torque constraint [mm/tooth]
r_c	cutting tool radius [mm]
v_m, v_k	position of disk m and disk k for deflection model
z	position of the elemental disk in respect to the bottom of the tool [mm]
E	Young's modulus [MPa]
F_r	reference force [N]
F_a	measured cutting force [N]

F_t, F_r, F_a	Cutting force components in tangential, radial and axial directions [N]
F_x, F_y, F_z	Cutting force components in the X, Y and Z directions [N]
$G_m(z)$	transfer function of the CNC
$G_p(z)$	transfer function of the cutting process
$G_c(z)$	transfer function of the CNC/cutting process
I	Inertia [mm4]
K_{tc}, K_{rc}, K_{ac}	Cutting force coefficients in tangential, radial and axial directions [N/mm2]
K_{te}, K_{re}, K_{ae}	Edge force coefficients in tangential, radial and axial directions [N/mm]
N	number of teeth on the cutting tool
P, P_{max}	Power and maximum power [hP] or [kW]
P_{ij}, Q_{ij}, R_{ij}, S_{ij}, T_{ij}, U_{ij}, Z_{ij}	Geometric constants for tooth j with respect to surface i
T, T_{max}	Torque and maximum torque [N.m]
T_f	tooth passing frequency [Hz]
V	Cutting speed [m/min]
α_n	normal rake angle [rad]
α_r	orthogonal rake angle [rad]
α_{xx}, α_{yy}	directional dynamic milling force coefficients
β_a	orthogonal friction angle [rad]
β_n	normal friction angle [rad]
τ_s	shear stress [MPa]
δ_y	deflection in y direction [mm]
ω_c	chatter frequency [rad/s]
ψ	helix angle [rad]

ι	chip flow angle [rad]
ϕ	tool angle [rad]
ϕ_c	pitch angle [rad]
ϕ_j	position of tooth j [rad]
$\phi_{st,i}$	entry angle, surface i [rad]
$\phi_{ex,i}$	exit angle, surface i [rad]
Λ	eigenvalue
Λ_I	imaginary part of the eigenvalue
Λ_R	real part of the eigenvalue

Chapter 1

Introduction

Milling is widely used by companies in the aerospace, automotive and mold and die industries. It is used to produce parts with simple or complex shapes as accurately as possible, in small or large volumes, and to remove material as rapidly as possible while maintaining tool and machine integrity. The milling tool path is created using CAD/CAM software. Common manufacturing practices in NC programming are usually based on the programmer's knowledge and experience, and tool proofing is done using trial and error methods. Over the last decades though, research in the area of milling has produced significant advancements in metal cutting mechanics, dynamics, modelling and simulation of the process. These projects are now being introduced in the industry and engineering practices are changing gradually.

Modelling and simulation of the milling process provide tools to evaluate and improve the selection of cutting parameters and the milling operation. Simulations include cutting forces, tool deflections, torque and power requirements, and chatter vibration stability check. On the other hand, the current milling process simulation systems process one set of specific cutting conditions at a time.

The objective of Virtual Milling is therefore to integrate in one system, milling process simulation and CAD/CAM, offering the possibility to not only simulate the milling process for one set of cutting conditions, but for the whole NC program. It offers several advantages to single cutting condition milling simulation. It allows the identification of critical locations on the part which require special attention in the NC programming. Also, it permits feedrate scheduling for the whole part and for various machining constraints, increasing machine performance, improving

machining cycle time and producing quality parts. It will also help to reduce the tool proofing time required before starting production. This time should be greatly reduced or eliminated.

This thesis studies the development of a Virtual Milling application for 2 1/2 D parts, including the milling simulation and feedrate scheduling. The thesis outline is as follows.

Chapter 2 is the literature review conducted in the areas of modelling of milling forces and Virtual Milling. The milling models developed to simulate cutting forces are first introduced. Research projects in the area of Virtual Milling are presented and the research objectives are stated.

Chapter 3 defines the milling process and describes in more details the analytical closed-loop milling force model used in the milling simulation. There are many constraints that limit the machining of metals, and milling simulation is relevant in this context. Two approaches for deflection calculations are presented. Cutting experiments were done to validate the models.

Chapter 4 presents the implementation of the Virtual Milling application. A new interface was developed and integrated in a CAD/CAM software for the selection of stable cutting conditions. Feedrate scheduling is then investigated. Two approaches were implemented in the scheme of the Virtual Milling application and they were compared with an existing online adaptive force control algorithm.

Conclusions and summary of the results are presented in chapter 5.

Chapter 2

Literature Review

2.1. Overview

Milling is one of the mostly used metal cutting process . In order to understand the physics of the process and increase its efficiency, many research projects have focused on cutting mechanics, modelling and simulation of the milling process. Virtual simulation of the process, i.e, Virtual Millling, is based on the integration in one system of milling process simulation and CAD/CAM capabilities to extract geometric information from the part model and the toolpath. First, the major contributions in the area of modelling of milling forces are presented. Then, past and current research in the area of Virtual Milling is covered. Finally, the research objectives of this project are formulated.

2.2. Modelling of Milling Forces

This section covers the modelling of milling forces. First, orthogonal and oblique cutting are introduced, then the two main force models and two approaches to identify cutting coefficients are described.

2.2.1. Orthogonal Cutting and Oblique Cutting

The cutting operations are divided into two types of operations: orthogonal cutting and oblique cutting. In orthogonal cutting, the straight cutting edge is perpendicular to the relative

motion of the tool with respect to the workpiece and two forces are generated on the cutting edge: feed force and tangential force. In the case of oblique cutting, the relative velocity of the work-piece is not perpendicular to the cutting edge anymore. For the milling operation, which falls into the category of oblique cutting, the inclination angle is equal to the helix angle of the cutter. Oblique cutting will produce 3 components of forces identified as tangential, radial and axial forces. It will be shown later that assumptions from the classical oblique cutting model can be used to simplify the calculations of cutting coefficients for milling using an orthogonal cutting database [18].

2.2.2. Cutting Force Models

Many research works have focused on the understanding of the force generation during the milling operation. The relationship between the uncut chip thickness and milling force was first reported by Koenigsberger and Sabberwal [29][34]. In this thesis, the main models based on the uncut chip thickness, average chip thickness model [42] and linear edge force model [11][42][46], are presented.

Average Chip Thickness Model

The average chip thickness model [42] relates the uncut chip thickness h to the cutting forces through the use of cutting coefficients. A force diagram is shown on figure 2.1. For an elemental slice of the milling tool at height z and for a specific cutting tooth j, the tangential $dF_{t,j}(\phi,z)$ and radial $dF_{r,j}(\phi,z)$ force components are given as :

$$dF_{t,j}(\phi, z) = K_t \cdot h_j(\phi, z) \cdot dz \tag{2.1}$$

$$dF_{r,j}(\phi, z) = K_r \cdot h_j(\phi, z) \cdot dz \tag{2.2}$$

where $h_j(\phi,z)$ is given by:

$$h_j(\phi, z) = s_t \sin\phi_j(z) \tag{2.3}$$

and where the angular position of tooth j at the height z, $\phi_j(z)$ is [36]:

$$\phi_j(z) = \phi + j\phi_c - \frac{\tan\psi}{r_c} z \tag{2.4}$$

ϕ being the angular position of the reference tooth, s_t : the feed per tooth, ϕ_c : the tooth angular spacing or pitch angle, ψ : the helix angle and r_c : the cutter radius. The cutting coefficients K_t and K_r are obtained by experiments and we will present two ways of identifying those coefficients in section 2.2.3. For a specific angular position ϕ of the tool, the total forces F_t and F_r are obtained by summing the elemental forces for all the teeth along the z axis, considering the sections of the cutting edges that are in cut.

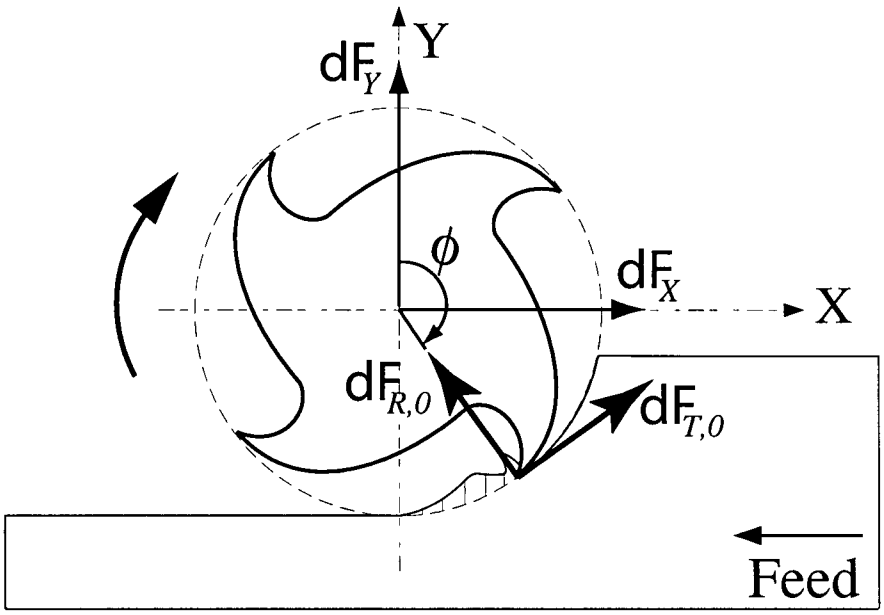

Figure 2.1 : Milling process - Force diagram.

Linear Edge Force Model

The average chip thickness model was improved by the addition of the edge force components following the work of Tlusty and MacNeil [42], Yellowley [46] and Armarego [11][13]. The edge force components represent the contact of the flank face of the tooth on the machined surface during the milling operation. The cutting coefficients K_{te} and K_{re} are added to the equations and the force model is given by Armarego [11] as :

$$dF_{t,j}(\phi, z) = (K_{tc} \cdot h_j(\phi, z) + K_{te})dz \tag{2.5}$$

$$dF_{r,j}(\phi, z) = (K_{rc} \cdot h_j(\phi, z) + K_{re})dz \tag{2.6}$$

The linear edge force model will be used in this project for the milling simulation.

2.2.3. Identification of Cutting Coefficients

Cutting coefficients can be identified using two approaches. The first approach is called mechanistic model. This approach consists in conducting a series of cutting tests on a milling machine with the milling tool for a same immersion condition but at several feedrates. Using linear regression on the experimental data, the cutting coefficients are identified, K_{tc} and K_{rc} being the slope of the corresponding linear regression curves and K_{te} and K_{re} the ordinates. This approach yields cutting coefficients which are specific to the cutting tool and the workpiece material [18].

The other approach relies on the orthogonal to oblique transformation proposed by Armarego [12]. Orthogonal cutting tests are first performed on a lathe with a series of inserts of different rake angles for several cutting speeds and feedrates. The cutting forces F_t and F_r are measured with a dynamometer and functions are statistically determined to represent shear stress, shear

angle and friction angle respectively, considering as well tool geometry and cutting conditions. The orthogonal to oblique cutting transformation is then used to calculate the cutting coefficients.

The first approach, mechanistic model, is useful and fast to identify cutting coefficients that are specific to one combination tool-workpiece material. On the other hand, in the case of multiple end mills used for the same material, the second approach will require more time for experiments but will produce a database that is suitable for all the end mills.

2.3. Virtual Milling

Available NC machining modules in CAD/CAM systems offer a wide selection of options to create complex tool paths. On the other hand, the selection of cutting conditions is left to the programmer, which specifies the cutting conditions according to his knowledge, his experience as well as machining data available in handbooks. Current CAD/CAM software systems do not model the machining process physics and do not provide tools to select appropriate cutting conditions in respect to the tool, cutting geometry, tool and workpiece materials, and machine tool limitations.

Milling process simulation is used to select stable cutting conditions. Tool geometry, workpiece material, cutting geometry, and dynamic parameters of the tool-machine system as well as the workpiece, are required to simulate the milling operation. When using a software like CutPro [10], developed in the Manufacturing Automation Laboratory at the University of British Columbia, the user is able to simulate cutting forces, torque and power requirements, tool vibrations and dimensional surface finish. A chart of the axial depth of cut as a function of the spindle speed can also be obtained for a specific width of cut, i.e. stability lobes, which provide the user with a graph of stable cutting conditions to choose from. This is generated for a specific set of cutting geometry, not for the whole part. The objective of Virtual Milling is therefore to simulate the process for the whole part, as well as to optimize the cutting conditions.

One of the first groups to work on a system that is aimed at simulating the milling process is Takata et al.[44] at the Osaka University. Their milling simulation system is based on an application interacting with a solid modeller. The geometric information required by the milling simulation is extracted from the solid modeller and the tool-workpiece intersections are calculated using the Z-buffer approach. Then, a discrete mechanistic model is used for force calculations and the elemental forces are computed along the edges of the tool and summed up. Tool displacements and regenerative effect are also considered in the calculation of the uncut chip thickness.

Their simulation system is used for both the prediction of cutting forces along the tool path as well as for the prediction of chatter vibrations. For chatter prediction, a simplified stability criterion proposed by Merrit [32] is used first. If this criterion is met, then the current case is stable and further calculations are not necessary. Otherwise, numerical simulations are performed and the occurence of chatter is identified by changes in cutting forces or tool displacements over several revolutions of the tool. However, as stated by the authors then, the simulation time is too long to be used in a practical application. In addition, Merrit's stability criterion is not suitable to use in milling since it is based on single point machining models.

Altintas and Spence [2][36][38] worked on a solid modeller based milling simulation system for 2 1/2 D workpiece. In this system, the workpiece is modelled using Constructive Solid Geometry (CSG) solid modelling. In order to calculate the static cutting forces as well as torque, power and tool deflections, a pre-processing step is done in which a semi-circular arc is swept in the feed direction and intersected with the part geometry in order to calculate the entry and exit angles of the cutter. With the immersion conditions, the cutting forces are calculated using an analytic closed form solution. Therefore, digital integration along the z axis is not necessary. The advantage of this method is a reduced computation time compared to methods using discretization of the tool along the z axis. The milling simulation also includes feedrate scheduling which is performed based on constraints such as maximum force, maximum power and torque, maximum tool

deflection and maximum chip load. This simulation system was developed for straigth paths and for cylindrical end mills only.

Altintas and Spence also developed a CAD assisted adaptive control [37]. This adaptive force control helps prevent force overshoots by feeding information to the controller ahead of time regarding sudden geometry changes so that the controller adjusts the feed before its actual occurrence. The algorithm uses an adaptive pole placement approach to maintain the peak cutting force to a reference force level. Experimental results showed that force overshoots were eliminated.

Spence [35] continued research in the area of milling process simulation and developed an application based on the ACIS Solid Modeler Kernel. The application is now based on B-Rep modelling. While the Z-buffer method offers advantages such as simplicity, robustness, relatively high computational time, the author suggests that Z-buffer approach is better fit to applications such as visual inspection of NC tool paths for collisions and for feedrate scheduling based on material removal rate. On the other hand, the B-Rep approach is more exact for calculations of tool-workpiece intersection, but the computational time is longer. Therefore, Spence et al. [39] worked on implementing methods to increase the computational speed of the B-Rep approach. They focused on parallel processing implementations, using round robin parallel processing, dual CPU, networked solutions and neighbor groups. The latter reduces the Boolean subtraction time through grouping of related primitives and gives better results than the round robin approach. They also worked on on-line monitoring and control of the milling process [35]. A new concept was also introduced : departure paths. The use of departure paths provides a way to remove the tool smoothly from the workpiece without leaving dwell marks on the part if the cutting conditions are generating high cutting forces and the controller is not able to adjust the feedrate accordingly. Once the tool is moved away from the part, the toolpath is reinitiated with appropriate cutting conditions.

Another group of researchers, Fussell and Jerard, also developed a milling process simulation system to optimize feedrates for 3-axis milling of sculptured surfaces using ball end mills[23][24][26][33]. They used a combination of off-line feedrate optimization schemes with on-line adaptive force control to maintain a peak force during end milling for safe, accurate and efficient machining. The feedrate optimization is based on constraints such as machine power, shank failure, tooth failure and surface finish. The addition of adaptive force control is to ensure that force overshoots are avoided. Also, the authors suggest that this approach will compensate for the inaccuracies caused by variations in the force prediction model or occurences that can not be predicted due to variations in material, tool condition, cooling fluid, tool runout, etc... Their system is also based on a Z-buffer representation of the geometric model for the tool-workpiece intersection calculations. The cutting force model is a discrete mechanistic model.

They tested two types of controllers : a division controller and an adjustable PI controller. Both controllers give better results than the use of off-line feedrate optimization only, but the adjustable PI controller is slower than the division controller. In average, for roughing, semi-finishing and finishing, the experimental results using the combination of off-line optimization and on-line control show a decrease in cutting times by about 15% when compared to cutting times obtained from "standard practice" NC toolpaths. However, on a practical point of view, the system used for on-line control includes a dynamometer. Dynamometers as well as many sensors are adequate for laboratory experiments, but they can not be used as is in an industrial context.

2.4. Research Focus

This project focuses on the simulation of the milling process for the whole part. Static cutting forces, torque and power, deflections are calculated all along the tool path. In order to do so, the intersection between the tool and workpiece, specified by entry and exit angles, is required. This is obtained from another application developed in the Manufacturing Automation Laboratory.

The second objective is to develop an interface to suggest the selection of stable cutting conditions at the level of the NC programming, i.e. in the CAD/CAM software. With the specifications of the workpiece material, width of cut, frequency response functions of the tool, stability lobes are generated. The NC programmer can therefore select appropriate cutting conditions for the milling operation.

The last part of this project consists in feedrate scheduling. Two approaches have been used, constraint-based feedrate scheduling and offline virtual adaptive force control. The latter approach was developed in a previous research project. These 2 approaches are compared with online adaptive generalized predictive control [3][9].

Chapter 3

Modelling of the Milling Process

3.1. Overview

The objectives of machining are to produce parts as accurately as possible in order to obtain the right geometry and to meet the specified part tolerances, but also on an economical aspect to remove excess material as rapidly as possible while avoiding damages to the cutting tool and the machine tool. To control the process, it is important to have the capabilities to simulate and control cutting forces, tool deflections, and torque and power requirements. Understanding the influence of the cutting parameters and the cutting geometry is also relevant in order to improve and optimize the milling operations. As an example, increasing the cutter immersion or the depth of cut may result in force overshoots and eventually in tool breakage. The prediction and avoidance of such occurences using milling simulation will help improve the milling process.

The following sections present the models used in the milling simulation. First, the milling operation is described. Second, constraints in the machining of metals are discussed as these are the reasons why milling simulation is relevant. Then, the basic concepts behind the calculations of tool-workpiece intersections required for the milling simulation are given. Following, the linear edge force model in an analytical closed-loop from is presented in more details. Then, two approaches for deflection calculations are stated. Finally, experiments were conducted to validate the models and the results are shown.

3.2. Milling Process

Milling is an intermittent cutting process. The cutter teeth are successively entering and exiting the workpiece and generating the finished surface at a direction normal to the feed. The workpiece is fed towards a rotating tool with a linear feed speed. In many milling machine configurations, the workpiece is mounted on a table moved by feed drives while the cutting tool is mounted in the stationary spindle shaft which rotates using the spindle motor.

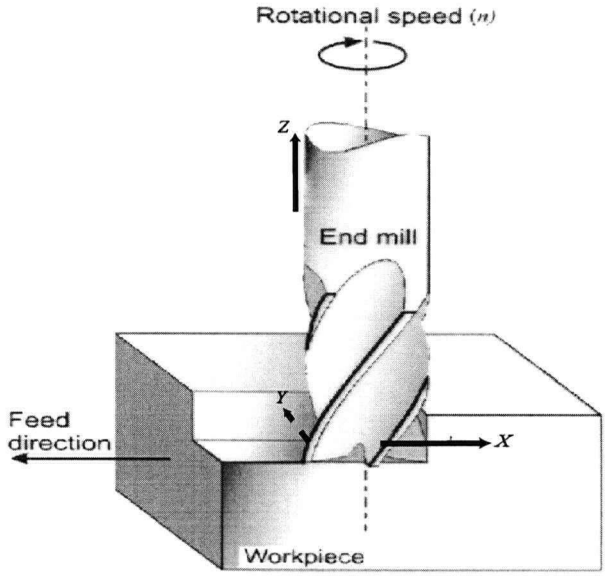

Figure 3.1 : Milling process.
Source : Manufacturing Automation, Altintas [9].

The programmed feedrate is relatively small compared to the spindle speed. Therefore, the assumption formulated by Martellotti [30] can be used : it states that the trochoidal path followed by the cutting teeth can be approximated as a circular motion. This commonly used assumption leads to the following equation for the chip thickness:

$$h(\phi) = s_t \sin\phi \tag{3.1}$$

Milling can be divided into two types of operations: face milling and peripheral milling. In face milling, the tool diameter is usually larger than the width of cut and the axial depth of cut is relatively small. Face mills are usually large tools with milling inserts. In peripheral milling, the cutting tool is smaller and the flank and tip of the tool are simultaneously used to remove material. There are several types of cutting tools for peripheral milling: cylindrical end mills, with or without a corner radius, tapered end mills, ball end mills, etc. Peripheral milling can also be divided in end milling and flank milling. It is used to machine pockets, slots, sculptured surfaces, etc.

Peripheral milling operations can also be divided into downmilling and upmilling. Figure 3.2 illustrates these 2 methods. The difference is in the way the chip is generated. In upmilling, the chip thickness is zero when the cutting tooth enters the material and it increases as the tool rotates. In downmilling, the chip thickness is the greatest when the cutting tooth enters the material and it becomes zero as it leaves the workpiece.

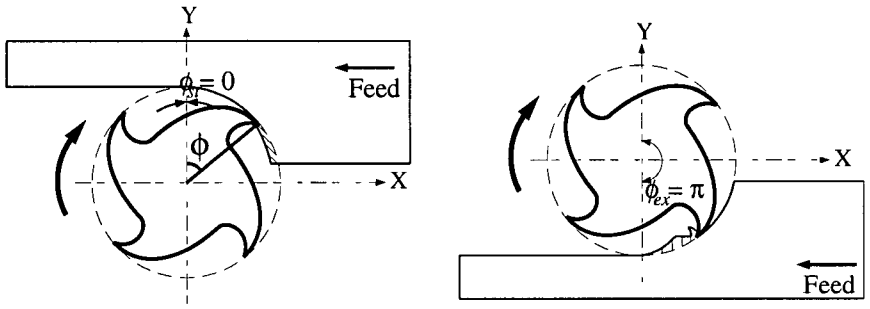

Figure 3.2 : Upmilling and downmilling.

Figure 3.3 shows a section of the cutting tool during a milling operation. As the cutting tool rotates, forces will vary in regards to the immersion of the cutting tooth and as a function of the chip thickness, axial depth of cut and the material properties. As mentioned earlier, the path of

each cutting tooth is often approximated as $h(\phi) = s_t \cdot \sin\phi$. In this work, we will use this equation for the chip thickness as it is sufficient for static cutting force calculations and for process planning purposes.

Cutting forces as shown on figure 3.3 are present all along the cutting edges which are in cut. Figure 3.4 shows the distribution of cutting forces along the cutting edges of an end mill. This distribution is a function of the cutting geometry, i.e. the axial and radial depths of cut, as well as the cutter geometry, i.e. the helix angle, cutter radius, and specific cutter geometry such as taper angle. The resultant tangential force, as well as the resultant planar force and the X, Y and Z forces are obtained by summing all the force components along the cutting edges.

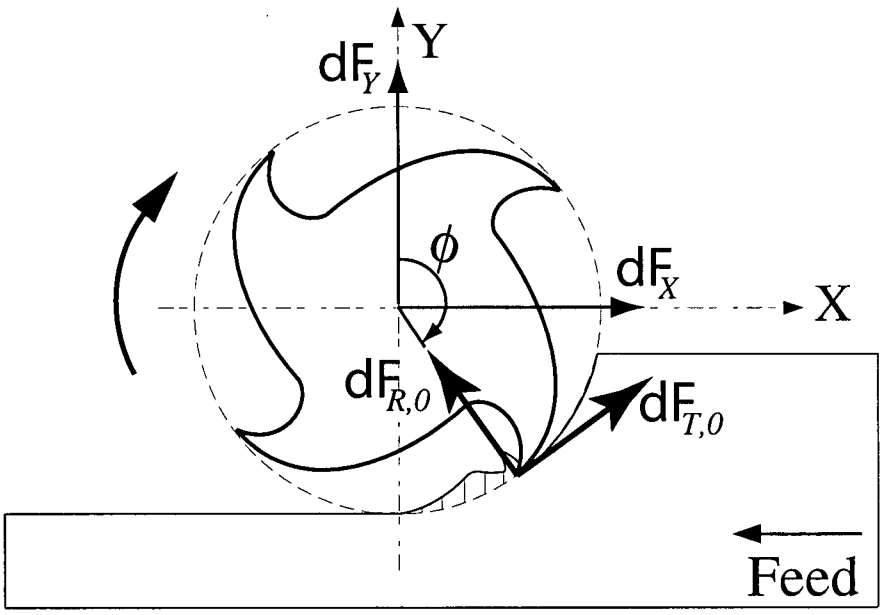

Figure 3.3 : Milling process - Force diagram.

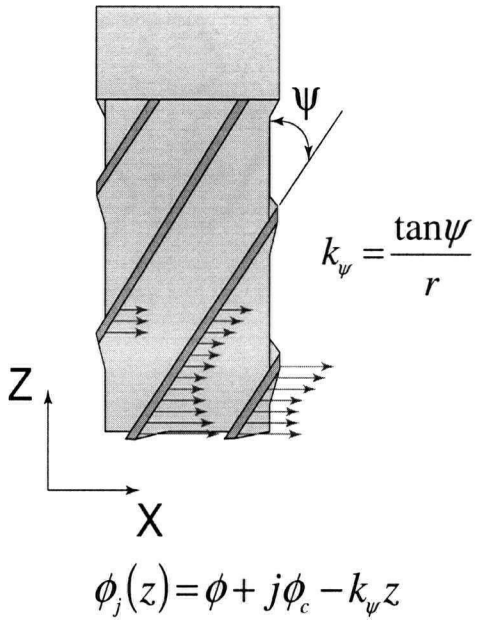

Figure 3.4 : Cutting forces along end mill.

3.3. Constraints

There are limitations to the milling process. The selection of cutting conditions has to be done considering the following constraints.

Machine tool dependent constraints

The spindle drives have limited capacity in terms of torque and power. It is therefore essential to check that the maximum torque and power do not exceed the spindle specifications.

Tool and workpiece dependent constraints

The chip load must not exceed the principal tensile stress in the cutting wedge beyond the ultimate tensile strength of the tool material. Also, the maximum static deflections left on the finished surface must be within the tolerance of the workpiece. Finally, the maximum resultant cutting force must be kept safely below a limit value to prevent fracture of the shank

3.4. Cutting tool - Workpiece Intersection

The cutting tool-workpiece intersection is the first step in the calculation of static cutting forces using the analytical model developed by Spence [36]. The geometry of helical end mills is first explained. Then, the intersection cases encountered during the milling operation are illustrated. In the last section, we discuss the calculation of the cutting tool - workpiece intersection and the calculation of entry and exit angles.

3.4.1. Helical End Mills

For helical end mills as shown on figure 3.4, the helix angle is such that the tooth engagement changes along the tool axis. The intersection of a given disk element along the z axis must be calculated. Therefore, the exact position of this disk element for each flute can be calculated. If we start with the bottom end points of the flutes, their positions are given by [36] :

$$\phi_j(0) = \phi + j\phi_c \qquad \text{for j=0,1,2,...} N-1 \tag{4.1}$$

where N is the number of teeth and $\phi_c = (2\pi)/N$ is the pitch angle. Then, at an axial depth of cut z for an elemental disk element, the position of tooth j is given by:

$$\phi_j(z) = \phi + j\phi_c - k_\psi z \qquad \text{for j=0,1,2,...}N-1 \tag{4.2}$$

As seen in the equation, in the case of end mills, the helix angle needs to be considered and the angular position along the z axis will vary with k_ψ, the lag angle. Therefore, k_ψ is defined as:

$$k_\psi = \frac{\tan\beta}{r_c} \tag{4.3}$$

where β is the helix angle and r_c the tool radius.

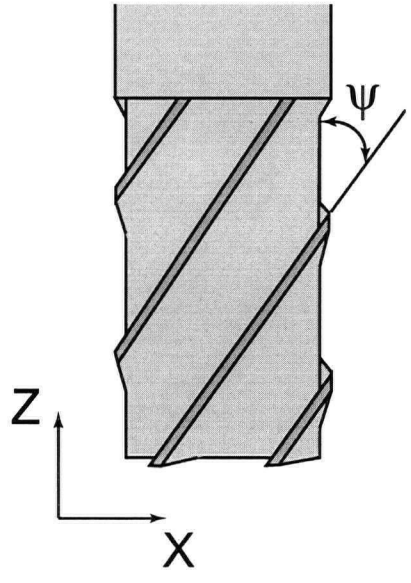

Figure 3.5 : Geometry of a helical end mill.

3.4.2. Intersection Cases

During the milling operation, as the cutting tool is rotating, each tooth engagement changes. The engagement of an elemental disk along a tooth will depend on the z position, the helix angle and the geometry of the workpiece.

There are five possible intersection cases, as identified by Spence [36]. Figure 3.6 illustrates these cases. As an example, the surface defined by the axial depth of cut a and between the entry angle ϕ_{st} and the exit angle ϕ_{ex} is the developed surface of a cut section of the workpiece shown in figure 3.6 and defined by $\phi_{st,0}$ and $\phi_{ex,0}$. On the graph, each line represents a possible intersection between a cutting edge and the workpiece. It is necessary to mention that these lines can not belong to the same cutting tool. In fact, the inclination of the cutting edges would all be the same as the helix angle is constant. Therefore, these lines would belong to different tools with different tool geometries.

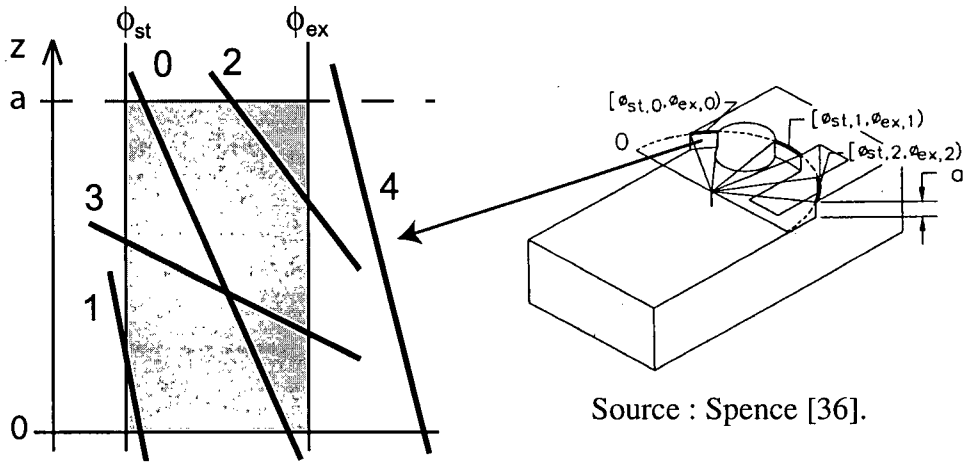

Source : Spence [36].

Figure 3.6 : Intersection cases and example of entry and exit angles.

As the tool rotates the cutting edge intersection case with the surface will change. Case 4 represents all the cases where cutting edges are out of cut. The identification of the intersection cases at each rotation of the cutting tool will be essential to calculate the geometric constants required for the cutting forces calculations.

3.4.3. Calculation of Entry and Exit Angles

The calculation of entry and exit angles is performed assuming the cutting tool geometry is a cylinder. The output will be a set of entry and exit angles. Figure 3.7 shows an example of entry and exit angles. In end milling, in most operations there is one in cut section, but it can occur that there are multiple engagements.

For the case of downmilling, the entry angle will be ϕ_{st}, depending on the workpiece geometry, and the exit angle will be π. For the case of upmilling, the entry angle is 0 and the exit angle is ϕ_{ex}, again depending on the workpiece geometry. In the case of slotting, the entry angle is 0 and the exit angle is π.

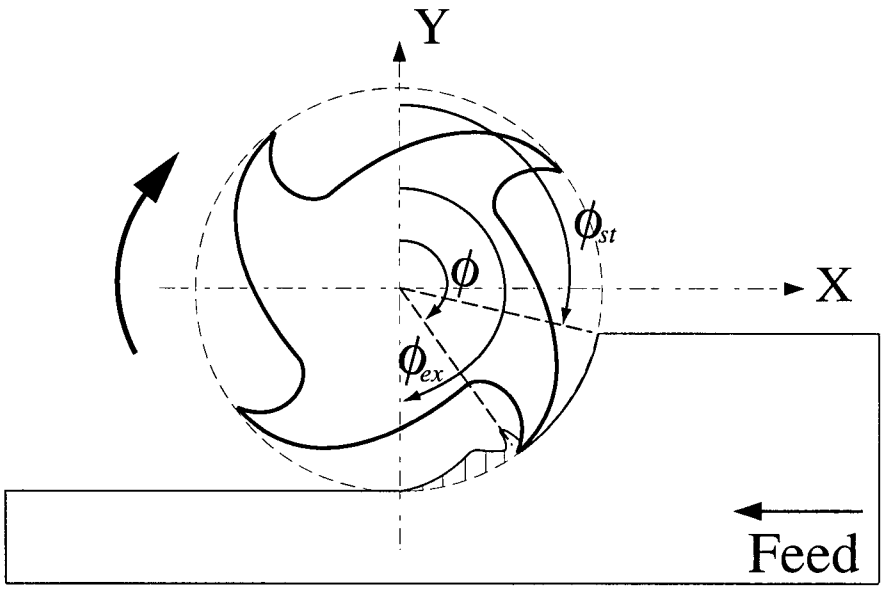

Figure 3.7 : Calculation of entry and exit angles.

3.5. Linear Edge Force Model - Analytical Closed-Loop Form

The linear edge force model was introduced in chapter 2. This model incorporates force components generated by the action of the chip on the rake face of the tool and the rubbing of the flank face on the new machined surface. As mentioned, the tangential, radial and axial force components are given as [36]:

$$dF_{t,j}(\phi, z) = (K_{TC} \cdot h_j(\phi, z) + K_{TE})dz$$

$$dF_{r,j}(\phi, z) = (K_{RC} \cdot h_j(\phi, z) + K_{RE})dz$$

$$dF_{a,j}(\phi, z) = (K_{AC} \cdot h_j(\phi, z) + K_{AE})dz$$

where $\phi_j = \phi + j\phi_c - k_\psi z$.

The equations are usually solved using integration along the z axis which translates in discretization in the z direction. In terms of computation time, this is a time consuming operation. For flat end mills, Spence [36] proposed to solve these equations as a closed-loop analytical force model. This approach has the advantage of eliminating the need to compute the forces along the z axis. Instead, the integration of the force components results in equations consisting of geometric terms and these terms are represented as geometric constants calculated for each specific position of the tool and are dependent on the intersection cases, as we will see later.

To obtain the forces in the machine directions, x, y and z, the force components are projected [36] :

$$dF_{x,j}(\phi_j(z)) = -dF_{t,j}\cos\phi_j(z) - dF_{r,j}\sin\phi_j(z) \tag{3.4}$$

$$dF_{y,j}(\phi_j(z)) = dF_{t,j}\sin\phi_j(z) - dF_{r,j}\cos\phi_j(z) \tag{3.5}$$

$$dF_{z,j}(\phi_j(z)) = dF_{a,j}(\phi_j(z)) \tag{3.6}$$

The cutting force components resulting from the intersection of a flute with a surface are obtained by integrating between the boundaries $z_{i,j,1}$ and $z_{i,j,2}$. These limits for each case are [36]:

Case 0 : $z_{ij1} = 0 \; z_{ij2} = a$

Case 1 : $z_{ij1} = 0 \; z_{ij2} = (1/k_\psi)[\phi + j\phi_c - \phi_{sti}]$

Case 2 : $z_{ij1} = (1/k_\psi)[\phi + j\phi_c - \phi_{exi}] \; z_{ij2}a = a$

Case 3 : $z_{ij1} = (1/k_\psi)[\phi + j\phi_c - \phi_{exi}] \; z_{ij2} = (1/k_\psi)[\phi + j\phi_c - \phi_{sti}]$

Case 4 : flute j is not cutting face i.

Integrating

$$F_{x,i,j}(\phi) = \int_{z_{i,j,1}}^{z_{i,j,2}} dF_{x,i,j}(\phi)dz \tag{3.7}$$

$$F_{y,i,j}(\phi) = \int_{z_{i,j,1}}^{z_{i,j,2}} dF_{y,i,j}(\phi)dz \tag{3.8}$$

$$F_{z,i,j}(\phi) = \int_{z_{i,j,1}}^{z_{i,j,2}} dF_{z,i,j}(\phi)dz \tag{3.9}$$

The analytical force equations become :

$$F_{x,ij}(\phi) = \frac{1}{k_\psi}\left[K_{TE}\sin\phi_j - K_{RE}\cos\phi_j + \frac{s_t}{4}[K_{RC}[2\phi_j - \sin 2\phi_j] - K_{TC}\cos 2\phi_j]\right]\Bigg|_{z_{ij1}}^{z_{ij2}} \tag{3.10}$$

$$F_{y,ij}(\phi) = \left(-\frac{1}{k_\psi}\right)\left[-K_{TE}\cos\phi_j - K_{RE}\sin\phi_j + \frac{s_t}{4}[K_{TC}[2\phi_j - \sin 2\phi_j] - K_{RC}\cos 2\phi_j]\right]\Bigg|_{z_{ij1}}^{z_{ij2}} \tag{3.11}$$

$$F_{z,ij}(\phi) = \frac{1}{k_\psi}[K_{AC}s_t\cos\phi_j - K_{AE}\phi_j]\Big|_{z_{ij1}}^{z_{ij2}} \tag{3.12}$$

Replacing ϕ_j in equations 3.10, 3.11 and 3.12 ,we can rewrite these equations :

$$F_{x,ij}(\phi) = \frac{1}{k_\psi}\left[K_{TE}S_{ij} - K_{RE}U_{ij} + \frac{s_t}{4}[K_{RC}T_{ij} - K_{TC}R_{ij}]\right]\Bigg|_{z_{ij1}}^{z_{ij2}} \tag{3.13}$$

$$F_{y,ij}(\phi) = \left(-\frac{1}{k_\psi}\right)\left[-K_{TE}U_{ij} - K_{RE}S_{ij} + \frac{s_t}{4}[K_{TC}T_{ij} - K_{RC}R_{ij}]\right]\Bigg|_{z_{ij1}}^{z_{ij2}} \tag{3.14}$$

$$F_{z,ij}(\phi) = \frac{1}{k_\psi}[K_{AC}s_tU_{ij} - K_{AE}\phi_jZ_{ij}]\Big|_{z_{ij1}}^{z_{ij2}} \tag{3.15}$$

where

$R_{ij} = \cos 2\phi_j$

$S_{ij} = \sin\phi_j$

$$T_{ij} = 2\phi_j - \sin 2\phi_j$$

$$U_{ij} = \cos\phi_j$$

$$Z_{ij} = \phi_j$$

The total forces are obtained by summing for all surfaces and all teeth :

$$F_x(\phi) = \sum_i \sum_j F_{x,ij} \tag{3.16}$$

$$F_y(\phi) = \sum_i \sum_j F_{y,ij} \tag{3.17}$$

$$F_z(\phi) = \sum_i \sum_j F_{z,ij} \tag{3.18}$$

The planar resultant force is obtained using the equation:

$$F(\phi) = [F_x^{\,2}(\phi) + F_y^{\,2}(\phi)]^{1/2} \tag{3.19}$$

3.5.1. Geometric Constants

Referring to figure 3.6, there are 5 possible intersection cases. The integration boundaries are z_{ij1} and z_{ij2}. For each intersection case, the geometric constants are defined as [2][36] :

Case 0: $z_{ij1} = 0 \;\; z_{ij2} = a$

$$P_{ij} = \cos(\phi + j\phi_c - k_\psi a)$$

$$Q_{ij} = \cos(\phi + j\phi_c)$$

$$R_{ij} = \cos 2(\phi + j\phi_c - k_\psi a) - \cos 2(\phi + j\phi_c)$$

$$S_{ij} = \sin(\phi + j\phi_c - k_\psi a) - \sin(\phi + j\phi_c)$$

$$T_{ij} = \sin 2(\phi + j\phi_c) - (2k_\psi a + \sin 2(\phi + j\phi_c - k_\psi a))$$

$$U_{ij} = \cos(\phi + j\phi_c - k_\psi a) - \cos(\phi + j\phi_c)$$

$$Z_{ij} = a$$

Case 1: $z_{ij1} = 0 \;\; z_{ij2} = (1/k_\psi)[\phi + j\phi_c - \phi_{sti}]$

$$P_{ij} = \cos\phi_{sti}$$

$$Q_{ij} = \cos(\phi + j\phi_c)$$

$$R_{ij} = \cos 2\phi_{sti} - \cos 2(\phi + j\phi_c)$$

$$S_{ij} = \sin\phi_{sti} - \sin(\phi + j\phi_c)$$

$$T_{ij} = \sin 2(\phi + j\phi_c) - (2(\phi + j\phi_c - \phi_{sti}) + \sin 2\phi_{sti})$$

$$U_{ij} = \cos\phi_{sti} - \cos(\phi + j\phi_c)$$

$$Z_{ij} = (1/k_\psi)(\phi + j\phi_c - \phi_{sti})$$

Case 2: $z_{ij1} = (1/k_\psi)[\phi + j\phi_c - \phi_{exi}] \;\; z_{ij2}a = a$

$$P_{ij} = \cos(\phi + j\phi_c - k_\psi a)$$

$$Q_{ij} = \cos\phi_{exi}$$

$$R_{ij} = \cos 2(\phi + j\phi_c - k_\psi a) - \cos 2\phi_{exi}$$

$$S_{ij} = \sin(\phi + j\phi_c - k_\psi a) - \sin\phi_{exi}$$

$$T_{ij} = 2(\phi + j\phi_c - k_\psi a) + \sin 2\phi_{exi} - (\sin 2(\phi + j\phi_c - k_\psi a) + 2\phi_{exi})$$

$$U_{ij} = \cos(\phi + j\phi_c - k_\psi a) - \cos\phi_{exi}$$

$$Z_{ij} = a - (1/k_\psi)(\phi + j\phi_c - \phi_{exi})$$

Case 3: $z_{ij1} = (1/k_\psi)[\phi + j\phi_c - \phi_{exi}]$ $z_{ij2} = (1/k_\psi)[\phi + j\phi_c - \phi_{sti}]$

$$P_{ij} = \cos\phi_{sti}$$

$$Q_{ij} = \cos\phi_{exi}$$

$$R_{ij} = \cos 2\phi_{sti} - \cos 2\phi_{exi}$$

$$S_{ij} = \sin\phi_{sti} - \sin\phi_{exi}$$

$$T_{ij} = 2\phi_{sti} + \sin 2\phi_{exi} - (\sin 2\phi_{sti} + 2\phi_{exi})$$

$$U_{ij} = \cos\phi_{sti} - \cos\phi_{exi}$$

$$Z_{ij} = (1/k_\psi)(\phi + j\phi_c - \phi_{sti}) - (1/k_\psi)(\phi + j\phi_c - \phi_{exi})$$

Case 4: flute j is not cutting face i

$$P_{ij} = Q_{ij} = R_{ij} = S_{ij} = T_{ij} = U_{ij} = Z_{ij} = 0$$

3.6. Maximum Torque and Power

Maximum torque is calculated using the following equation:

$$T_{max} = F_{t,max} \times r_c \tag{3.20}$$

The tangential force F_t is calculated analytically using geometric constants.

$$F_{t,ij}(\phi) = \int_{z_{ij1}}^{z_{ij2}} dF_{t,j}(\phi)dz \tag{3.21}$$

The tangential force component was given in equation 3.4:

$$dF_{t,j}(\phi, z) = (K_{TC} \cdot h_j(\phi, z) + K_{TE})dz$$

$$F_{T,ij}(\phi) = \int_{z_{ij1}}^{z_{ij2}} (K_{TC} \cdot s_t \sin\phi_j(z) + K_{TE})dz$$

$$F_{T,ij}(\phi) = -K_{TC}s_t\left[\frac{1}{k_\psi}(\cos(\phi + j\phi_c - k_\psi z_{ij2})) - \frac{1}{k_\psi}(\cos(\phi + j\phi_c - k_\psi z_{ij1}))\right] + (-K_{TE})[z_{ij2} - z_{ij1}]$$

$$F_{T,ij}(\phi) = \left(-\frac{K_{TC}}{k_\psi}\right)s_t U_t - K_{TE}Z_t \tag{3.22}$$

$$F_t(\phi) = \sum_i \sum_j F_{t,ij} \tag{3.23}$$

Once the maximum torque is found, the maximum power in hP is calculated using

$$P_{max} = \frac{T_{max} \cdot n}{745.7}(hP) \tag{3.24}$$

where n is the spindle speed expressed in rad/s.

3.7. Deflection Models

In this application, the assumption is that tool deflections are solely the result of cutting forces acting on the flexible cutter. Parameters such as run-out, deflection of the workpiece are therefore not considered. The model assumes static deflection of the cutting tool.

Two approaches are used to calculate deflections. For the calculation of deflections along the tool, static deflection is calculated using the cantilevered beam formulation for forces applied all

along the tool. For the calculation of maximum deflection, an analytical approach is used. In this approach, the force is applied on the tool at halfway the axial depth of cut. It was demonstrated that this simplified, concentrated maximum normal force deflection model is appropriate for rigid parts [36].

3.7.1. Deflection along the Tool

We assume that the cutting force is applied at the tool tip of the endmill and that it causes the tool to deflect statically. The deflection is given by:

$$\delta_y = \frac{F_y}{k_t} \tag{3.25}$$

where $k = \frac{3EI}{l^3}$ and $I = \frac{\pi d^4}{64}$.

We observe that the surface generation is not the same for upmilling and downmilling. In the case of upmilling, the cutter teeth enter in the material and cause overcutting. In downmilling, the forces acting on the tool push it out of the workpiece therefore resulting in undercutting.

The finished surface is generated by the section of the tooth that is in contact with it. In upmilling, this occurs at $\phi_{st} = 0$, while in downmilling at $\phi_{ex} = \pi$. The surface is either generated by a single contact point for a position ϕ_j of the tool, or by many contact points. As formulated earlier in equation 4.2, the angular position of tooth j for a depth of cut z is given by :

$$\phi_j(z) = \phi + j\phi_c - k_\psi z \qquad \text{for j=0,1,2,...} N-1$$

where $k_\psi = \frac{\tan\beta}{r_c}$.

Therefore, the contact points for upmilling and downmilling are derived by setting $\phi_j = 0$ for upmilling and $\phi_j = \pi$ for downmilling:

$$z_{upmilling}(\phi) = \frac{\phi + j\phi_c - \pi}{k_\psi} \tag{3.26}$$

$$z_{downmilling}(\phi) = \frac{\phi + j\phi_c}{k_\psi} \tag{3.27}$$

The cutter is divided into M small disk elements. The axial depth of cut is a, so the height of one element is $\Delta z = a/M$. If a large number of elements is used, the influence of the helix angle can be neglected.

The differential cutting force at element m is [9] :

$$\Delta F_{y,m}(\phi) = K_t s_t \Delta z \sum_{j=0}^{N-1} [\sin\phi_j(z) - K_r \cos\phi_j(z)] \sin\phi_j \tag{3.28}$$

The deflection at z_k caused by the force applied at element m is obtained using the cantilevered beam equation [17] :

$$\delta_y(z_k, m) = \begin{cases} \frac{\Delta F_{y,m} \nu_k^2}{6EI}(3\nu_m - \nu_k) \\ \frac{\Delta F_{y,m} \nu_m^2}{6EI}(3\nu_k - \nu_m) \end{cases} \tag{3.29}$$

where $\nu_k = l - z_k$ and $\nu_m = l - z_m$.

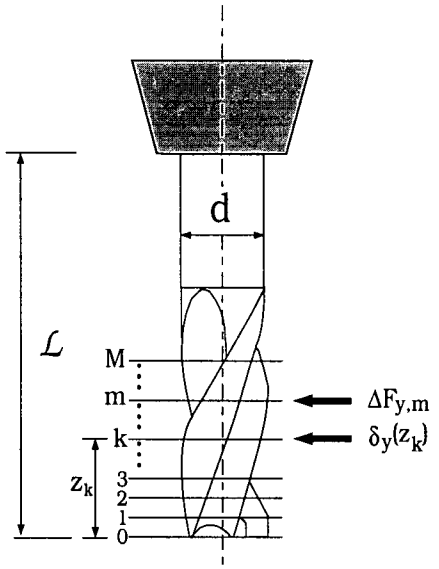

Figure 3.8 : End mill - Static deflection model.
Source : Manufacturing Automation, Altintas [9].

3.7.2. Maximum Deflection

Deflection of the tool will cause overcutting in upmilling and undercutting in downmilling. Both situations, the deflection is maximum when the normal force F_y reaches its maximum and there is a contact point in cut.

As proposed by Spence [36], we assume the maximum deflection occurs at the tool tip and that the force distribution can be approximated as the resultant force in y being applied at one point corresponding to half of the axial depth of cut. From figure 3.9, we observe that:

$$A = L - a/2 \tag{3.30}$$

and the maximum deflection is :

$$\delta_{y,\,max} = \frac{F_{y,\,max} A^2 (A - 3L)}{6EI} \tag{3.31}$$

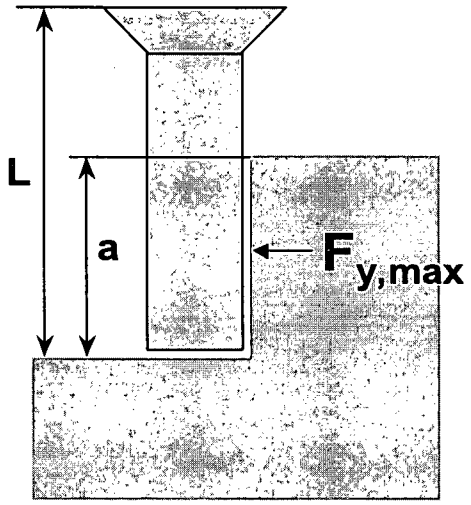

Figure 3.9 : End mill deflection model.

3.8. Validation of the Milling Force Model

3.8.1. Test Part and Set-Up

A test part featuring 3 different pockets, figure 3.11, was designed to verify the accuracy of the prediction of cutting forces. The test consists in machining the three pockets and to measure the cutting forces along the toolpath. These 3 pockets allow for different sets of entry and exit angles along the tool path as well as cases where there are more than one set of entry and exit angles for the same tool position. Also, the direction of the cutting forces vary along the tool path.

The cutting tool is a two-flute cylindrical end mill with a 12 mm diameter, a helix angle of 30 degrees, and a rake angle of 8 degrees. We assumed no corner radius. Finally, the workpiece is mounted on a Kistler dynamometer with sensors to measure F_x, F_y and F_z. The cutting forces are recorded using the MAL-DAQ module from CutPro [10].

The depth of cut is 4 mm, the spindle speed is 2500 rpm and the feedrate is 500 mm/min. Figure 3.10 shows the toolpath. For the rectangular pocket, a helical inward toolpath was used with plunging entrance of the tool in the center of the pocket. For the triangular toolpath, a helical inward toolpath was used as well. For the circular toolpath, an helical outward toolpath was used.

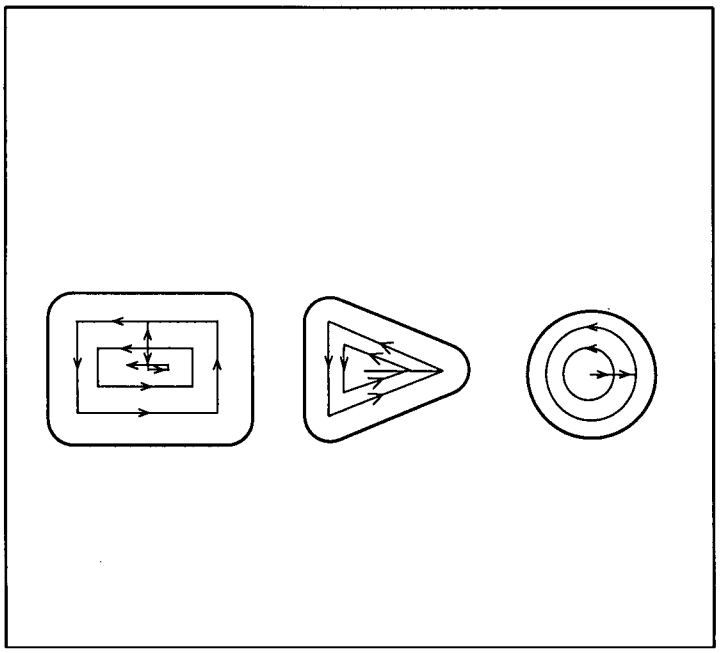

Figure 3.10 : Toolpath.

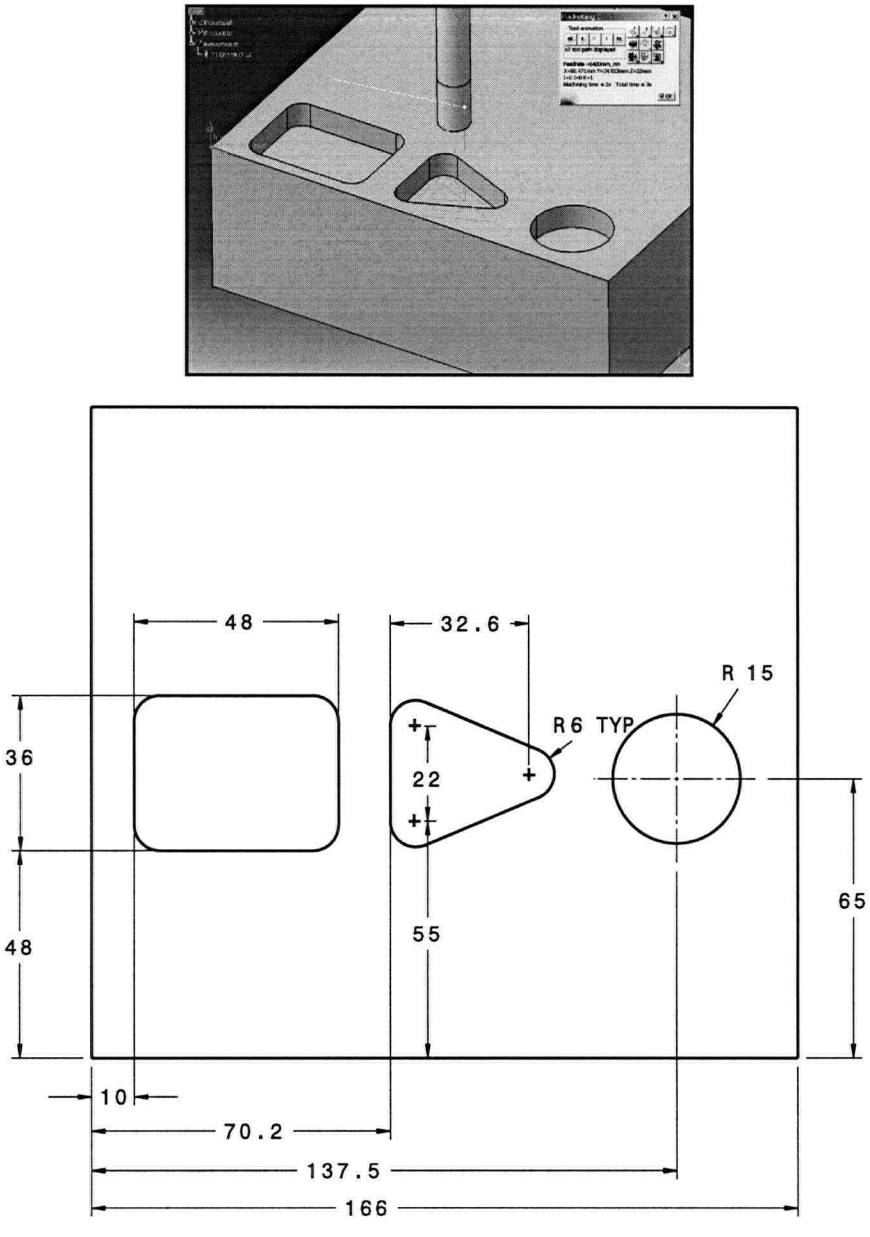

Figure 3.11 : Test part with three features and dimensions.

The workpiece material is Al7050-T7451. The cutting coefficients for this material are obtained using an orthogonal to oblique cutting model presented by Budak, Altintas and Armarego [18].

Orthogonal to Oblique Cutting Transformation

The cutting coefficients are transformed from shear stress, shear angle, friction angle and edge coefficients measured in orthogonal cutting tests using a classical oblique cutting model. It was found that this material behavior is a function of chip thickness and spindle speed. The cutting coefficients are therefore updated along the tool path as the chip thickness varies.

The relations for the shear stress τ_s , shear angle ϕ_n , friction angle β_n and the edge coefficients are for Al7050-T7451 :

$$\tau_s = 297.0528 + 1.0474 \cdot \alpha_n$$

$$\phi_n = 24.2013 + 36.6678 \cdot h + 0.0049 \cdot V + 0.2995 \cdot \alpha_n$$

$$\beta_n = 18.7883 - 6.7008h - 0.0076V + 0.2581\alpha_n$$

$$K_{TE} = 23.4071 - (0.0014 \cdot V) - (0.2555 \cdot \alpha_n \cdot 180/\pi)$$

$$K_{RE} = 35.1607 - (0.0011 \cdot V) - (0.5076 \cdot \alpha_n \cdot 180/\pi)$$

$$K_{AE} = 0$$

where α_n is the normal rake angle in degrees, $h[mm]$ is the chip thickness and V is the cutting speed in [m/min]. In the classical orthogonal to oblique cutting transformation model, the following assumptions are made [12] :

1) the orthogonal shear angle ϕ_c is equal to the normal shear angle ϕ_n in oblique cutting;

2) the normal rake angle α_n is equal to the orthogonal rake angle α_r;

3) the chip flow angle ι is equal to the oblique cutting angle η;

4) the friction coefficient β_a and the shear stress τ_s are the same in orthogonal and oblique cutting for a combination of speed, chip load and tool-material pair.

The equations for the cutting coefficients are [12] :

$$K_{TC} = \frac{\tau_s}{\sin\phi_n} \cdot \frac{\cos(\beta_n - \alpha_n) + \tan\iota \cdot \tan\eta \cdot \sin\beta_n}{c} \tag{3.32}$$

$$K_{RC} = \frac{\tau_s}{\sin\phi_n \cos\iota} \cdot \frac{\sin(\beta_n - \alpha_n)}{c} \tag{3.33}$$

$$K_{AC} = \frac{\tau_s}{\sin\phi_n} \cdot \frac{\cos(\beta_n - \alpha_n)\tan\iota - \tan\eta \cdot \sin\beta_n}{c} \tag{3.34}$$

where $c = \sqrt{\cos^2(\phi_n + \beta_n - \alpha_n) + \tan^2\eta \cdot \sin^2\beta_n}$.

3.8.2. Transformation to XYZ Cartesian System

During milling simulation, the forces are first calculated in their local axis system. The X and Y forces must be transformed to obtain forces in the machine X and Y directions, as shown in figure 3.12, the Z direction being the same. They are projected as follows:

$$\left[dF_x \; dF_y\right]' = [T]\left[dF_{x,\,local} \; dF_{y,\,local}\right]' \tag{3.35}$$

$$\text{where T is } [T] = \begin{bmatrix} \cos\theta & -\sin\theta \\ \sin\theta & \cos\theta \end{bmatrix} \tag{3.36}$$

where θ is the angle between the local coordinate system and the machine coordinate system.

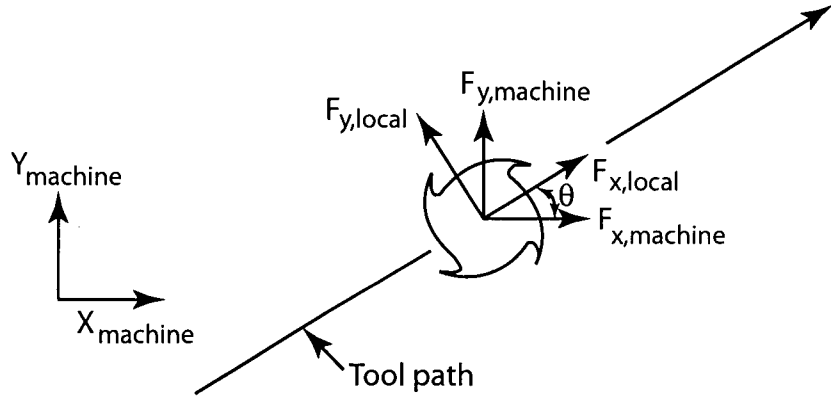

Figure 3.12 : Transformation of forces to machine coordinate system.

3.8.3. Simulation and Experimental Results

The envelope of the experimental and simulated results are presented for the X, Y , Z and resultant cutting forces for each part pocket in figures 3.13 to 3.18. From the results, we can make the following observations:

1) For the rectangular and triangular pockets, the trend of the simulated results generally follow the experimental results, except for the resultant force and the Z force for the rectangular pocket. The resultant force being the combination of X and Y results, this is explained by the fact that we are adding the slight deviations from both curves. In the case of the Z force, there is an offset of about 50 N that is not observed later during the machining of the two other pockets.

2) The experimental results exhibit a magnitude that is higher than the simulated results by about 50 N, which is an error of about 10%. The results present noise and drift from the measurement equipment, but this deviation is probably due to the material cutting coefficients.

The analysis of the results shows that the milling force model is accurate.

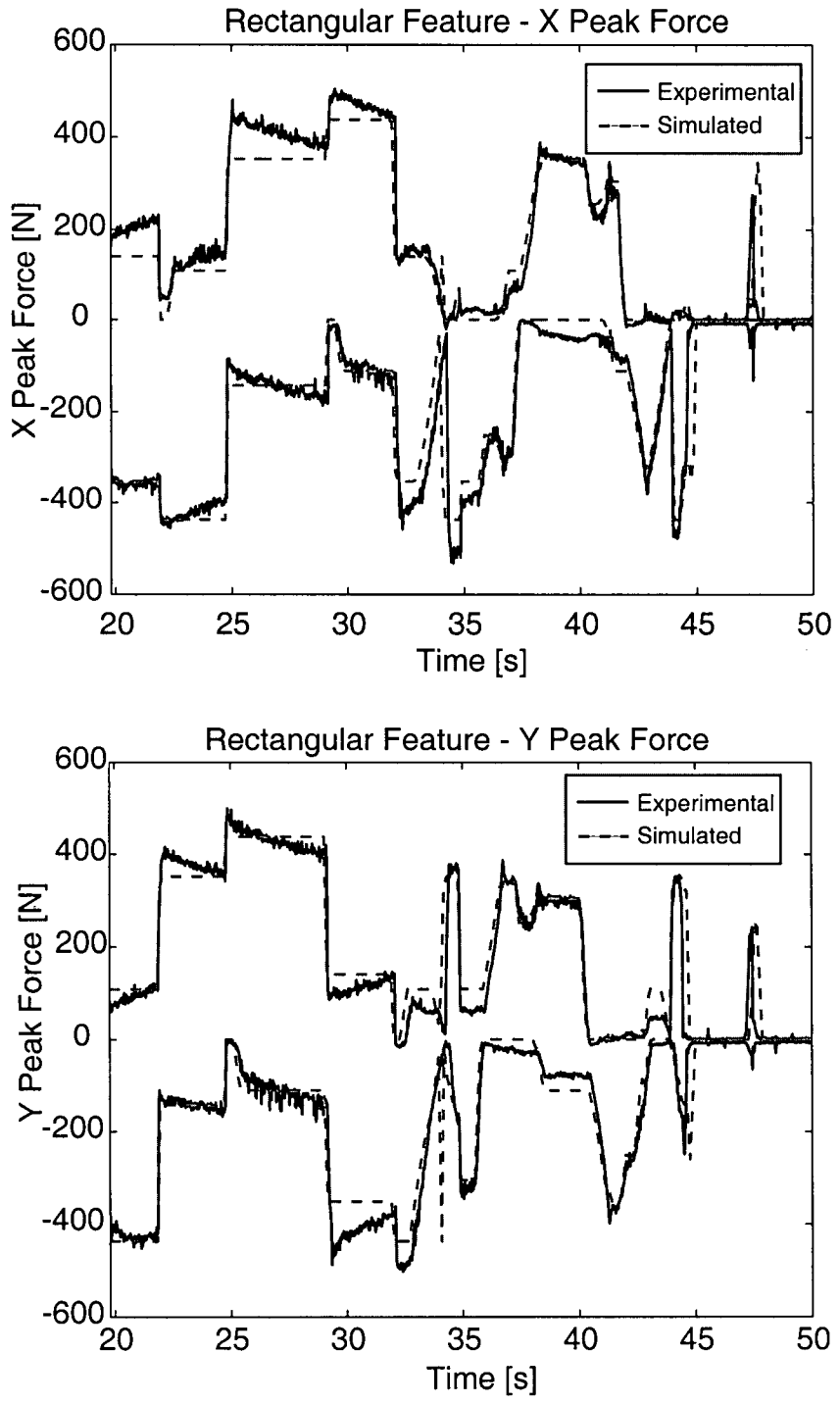

Figure 3.13 : Envelope for the X and Y cutting forces - Machining of the rectangular pocket.

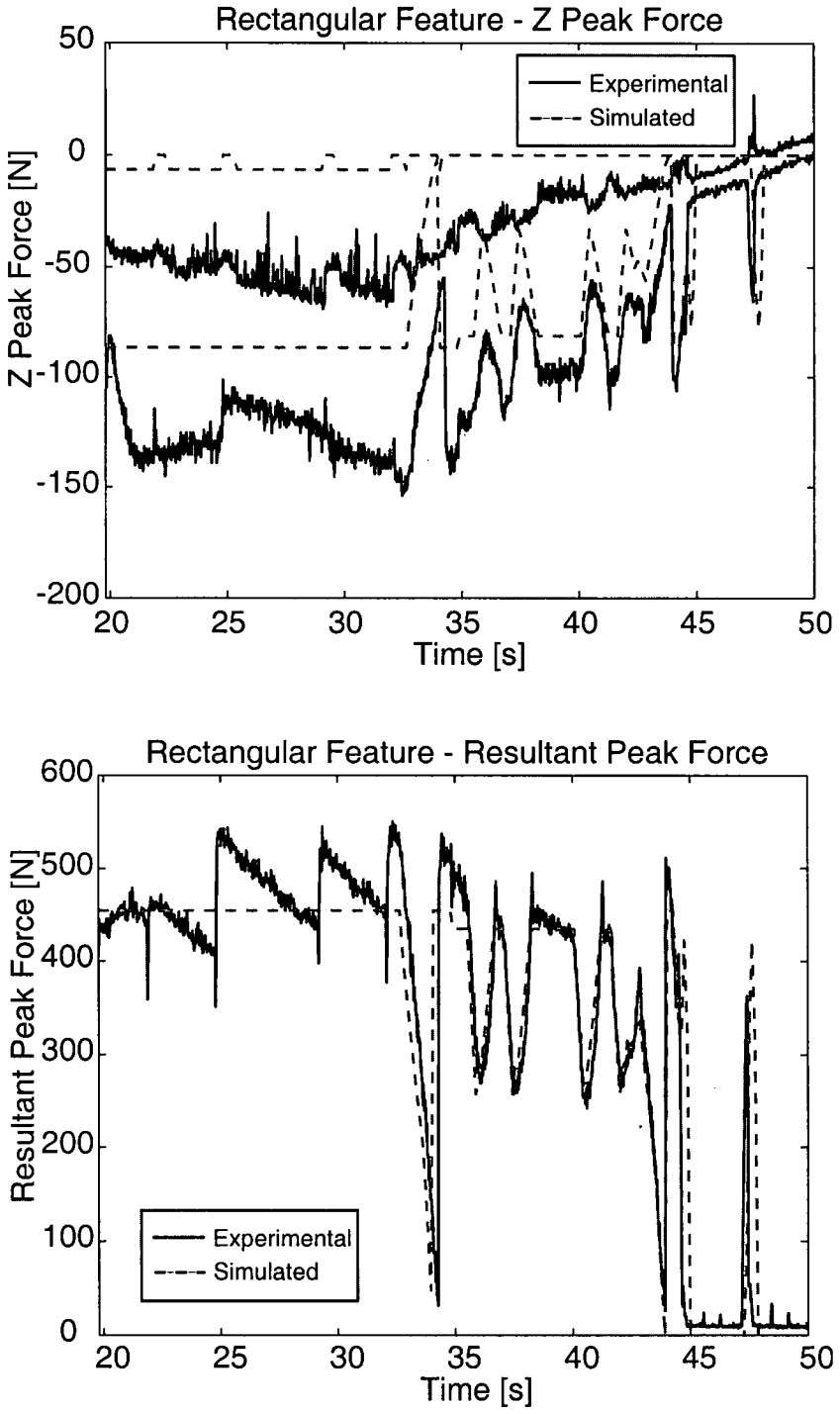

Figure 3.14 : Envelope for the Z cutting forces, and resultant cutting forces - Machining of the rectangular pocket.

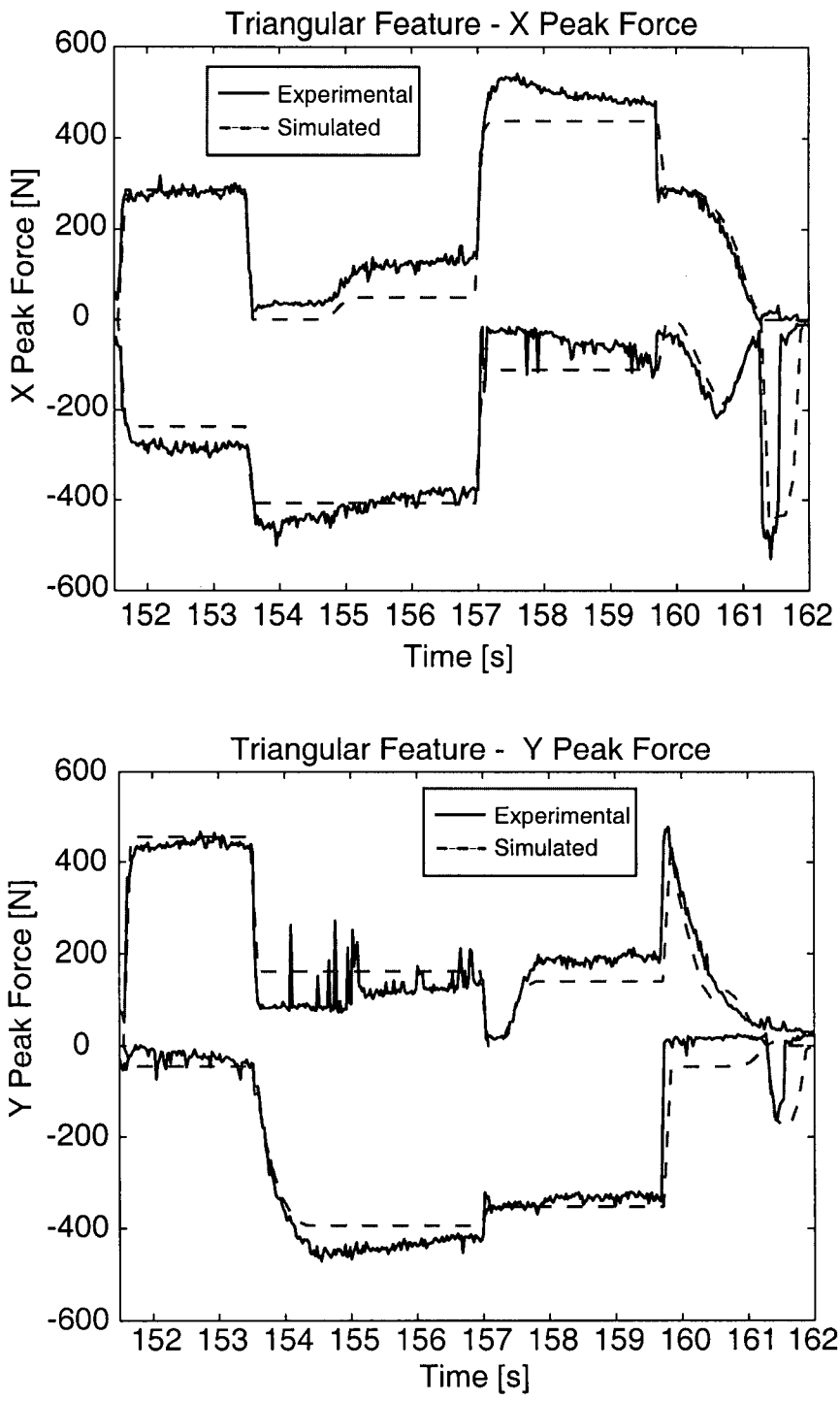

Figure 3.15 : Envelope for the X and Y cutting forces - Machining of the triangular pocket.

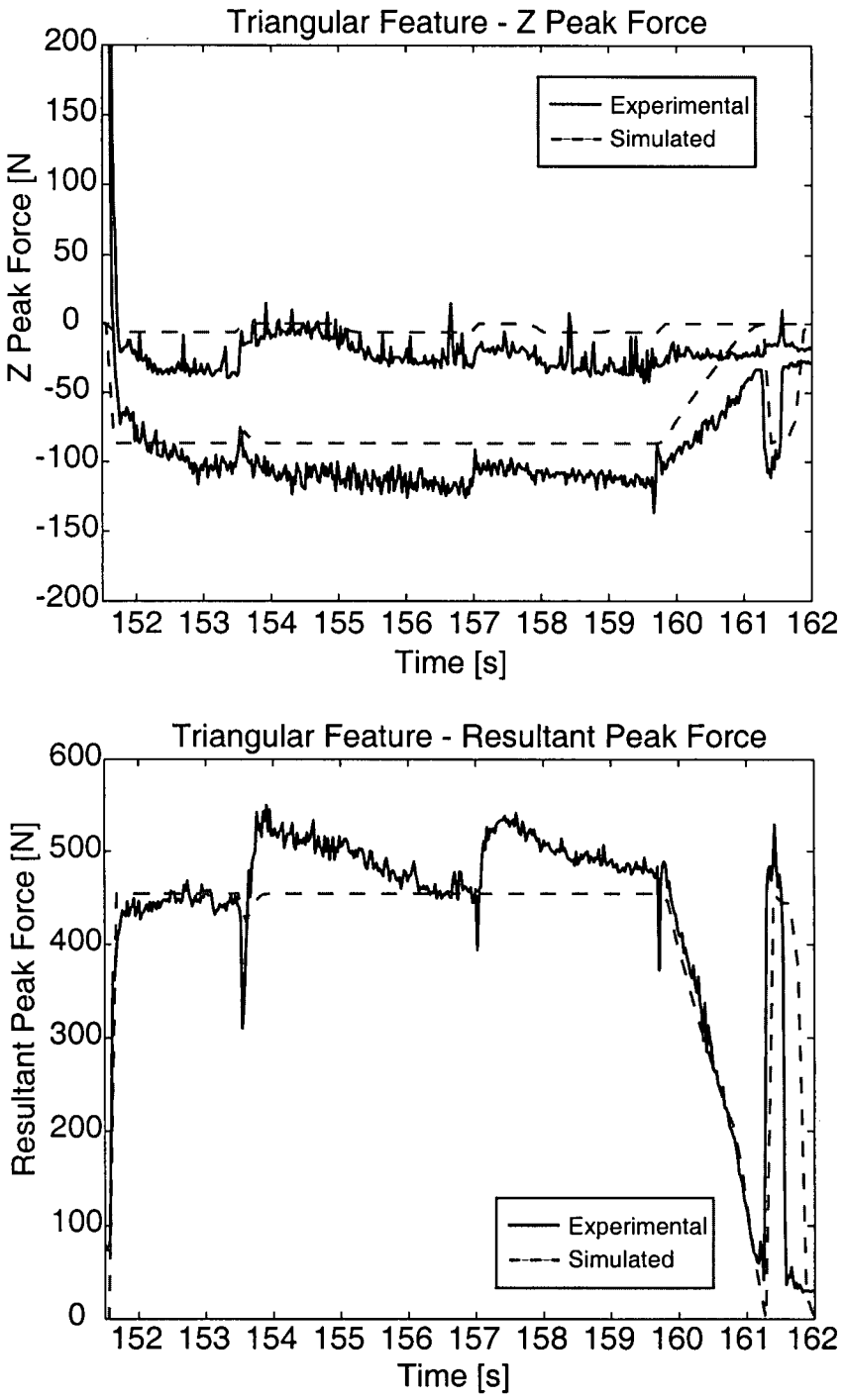

Figure 3.16 : Envelope for the Z cutting forces, and resultant cutting forces - Machining of the triangular pocket.

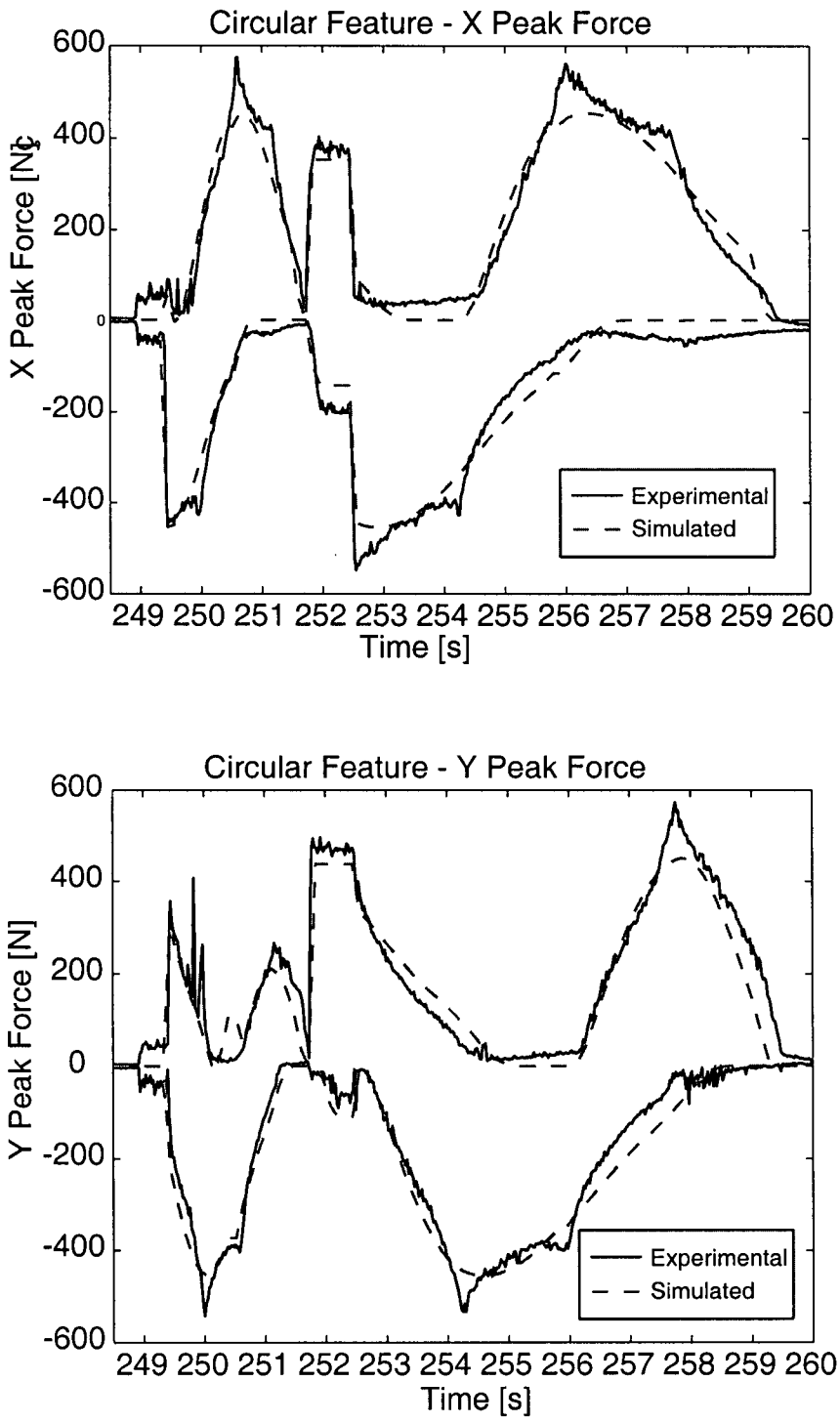

Figure 3.17 : Envelope for the X and Y cutting forces - Machining of the circular pocket.

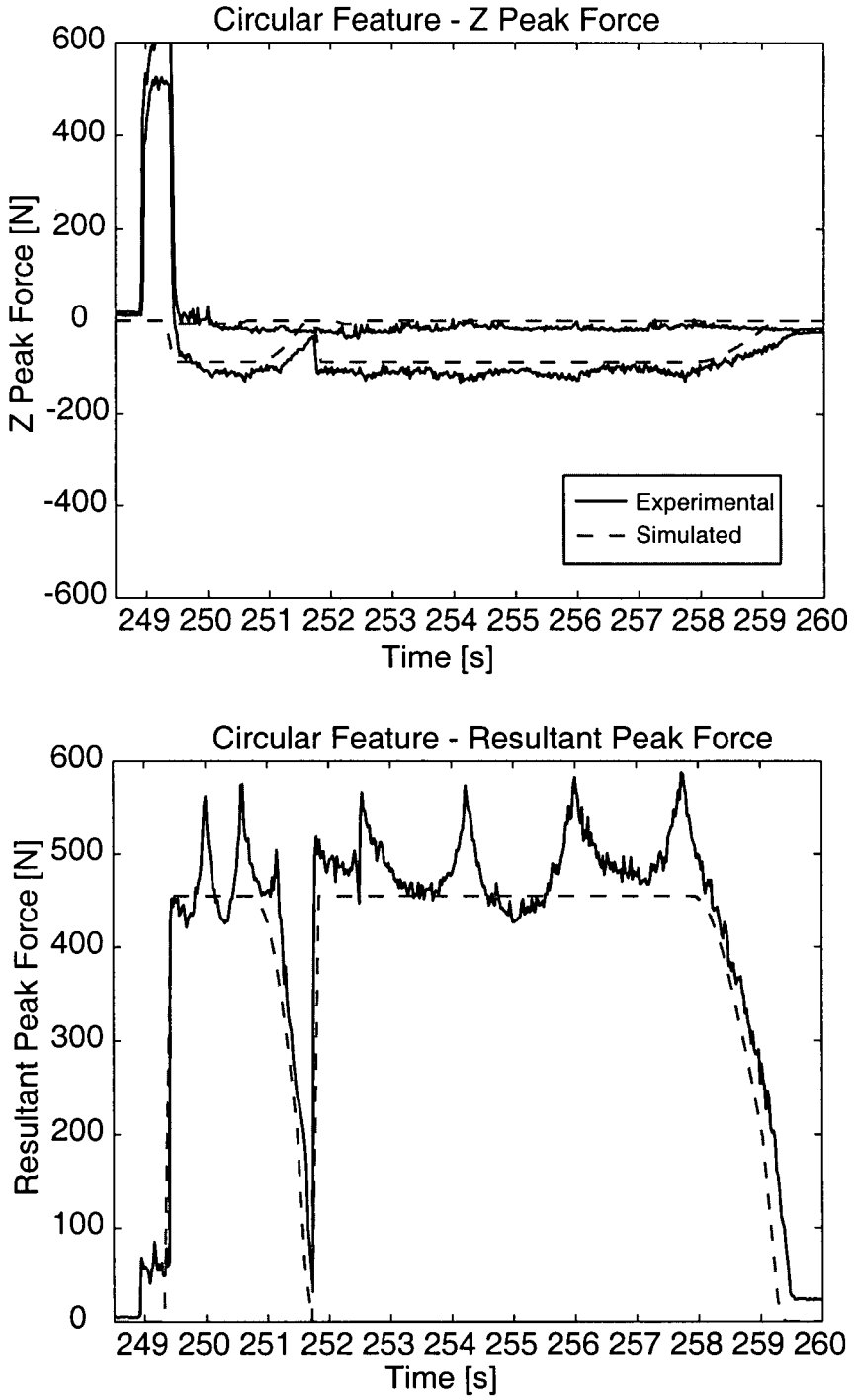

Figure 3.18 : Envelope for the Z cutting forces, and resultant cutting forces - Machining of the circular pocket.

Chapter 4

Virtual Milling Implementation

4.1. Overview

In chapter 3, the details of the milling simulation were given. In this chapter, the implementation of the milling simulation within the framework of the Virtual Milling project is presented. Virtual Milling offers several advantages to single cutting condition milling simulation. With Virtual Milling, the milling simulation is done for the whole part which allows the NC programmer to identify critical situations occuring during the operation. Also, feedrate scheduling and optimization is performed for the whole part and for various machining constraints, therefore maximizing machine performance, reducing cycle time and producing quality parts. Another major advantage of Virtual Milling is that the time spent on the machine tool to improve the NC program could be greatly reduced, if not eliminated.

The overall application is presented in the first sections, with the details of the interface developed for the selection of cutting conditions in CAD/CAM software, as well as the type of input required and the flowchart of the application. The following sections are dedicated to feedrate scheduling. Three approaches are used and experiments are conducted to validate the models and compare these approaches.

4.2. Virtual Milling Application

The flowchart shown in figure 4.1 illustrates the steps for the Virtual Milling project. The software components are the following:

- New interface in the CAD/CAM software for the selection of cutting conditions;
- CAD/CAM system to create the workpiece geometry and the NC tool path;
- Application developed in ACIS to calculate tool-workpiece intersection;
- Milling process simulation;
- Feedrate scheduling.

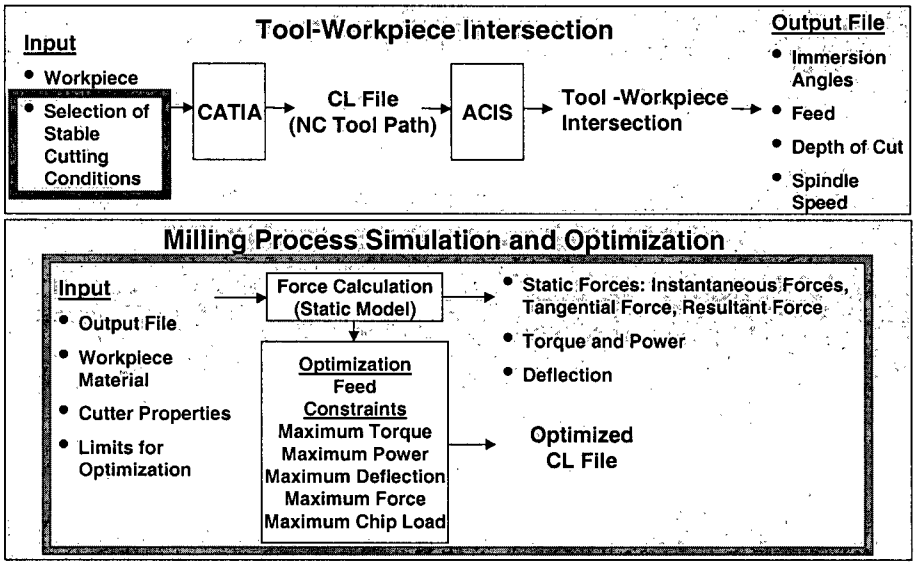

Figure 4.1 : Virtual Milling flowchart.

4.3. Selection of Cutting Conditions in CAD/CAM Software

During the creation of NC tool paths, the programmer must specify cutting conditions such as spindle speed, feedrate and depths of cut. Available CAD/CAM software do not provide tools for the selection of these cutting conditions. Most commercial NC packages offer interfaces where cutting parameters are entered but there is no knowledge or help available specifically for the selection of cutting conditions. The programmer therefore defines cutting conditions based on his knowledge and experience, and/or on information available in handbooks.

The proposed system integrates knowledge for the selection of these parameters. This is a new feature added to CAD/CAM software and it is the first step in the Virtual Milling. It allows for the selection of stable conditions for spindle speed, depth of cut and width of cut. The NC programming is done using these selected conditions and will therefore lead to stable operation. The feedrate is first selected using data available from tool manufacturers or handbooks, but will later be optimized in Virtual Milling using milling simulation and feedrate scheduling techniques. This part is presented in section 4.4.

To illustrate this idea, a new interface is developed and integrated in CATIA, a widely used commercial CAD/CAM software, especially by companies in the aerospace industry and in the automotive industry. The purpose of this new interface is to display stability lobes for specific tool and workpiece material combination and for a given width of cut during the NC programming. The programmer is then able to select the appropriate set of spindle speed and axial depth of cut to ensure stable cutting operation. The following sections introduce the theory of stability

lobes, and describe the requirements and functionalities of the system, as well as present the interface developed specifically in CATIA.

4.3.1. Stability lobes

Chatter vibrations are caused by a self-excitation mechanism in the generation of chip thickness during the milling operation. One of the structural modes of the tool-workpiece-machine system is first excited by cutting forces. The machined surface presents oscillations. The succeeding tooth is also oscillating due to the vibrations, therefore generating an oscillatory chip thickness. The chip thickness being oscillatory, the cutting forces become oscillatory as well. The self excited cutting system becomes unstable, and chatter vibrations grow until the tool jumps out of the cut or breaks under the excessive cutting forces. Thus, the chatter vibrations continue to be the major limiting factor in increasing the metal removal rates of the machine tools. [9]

In order to avoid conditions where chatter vibrations would develop, many researchers have worked in this area. Tlusty [41] and Tobias [43] first presented stability theory for orthogonal cutting. Merrit [32] also presented Nyquist stability based solution. Altintas and Budak [8] later presented an analytical solution applicable to the milling operation. This solution is used here to generate stability lobes. The reader should refer to [8],[9] for more details about the theory and equations.

The analytical stability lobes are obtained from the following characteristic equation [8][9]:

$$a_0\Lambda^2 + a_1\Lambda + 1 = 0 \tag{4.1}$$

where

$$a_0 = \Phi_{xx}(i\omega_c)\Phi_{yy}(i\omega_c)(\alpha_{xx}\alpha_{yy} - \alpha_{xy}\alpha_{yx}) \tag{4.2}$$

$$a_1 = \alpha_{xx}\Phi_{xx}(i\omega_c) + \alpha_{yy}\Phi_{yy}(i\omega_c). \tag{4.3}$$

Φ_{xx} and Φ_{yy} are the direct transfer functions in the x and y directions. α_{xx} and α_{yy} are the directional dynamic milling force coefficients. ω_c is the chatter frequency. The eigenvalue Λ is then solved by :

$$\Lambda = -\frac{1}{2a_0}(a_1 \pm \sqrt{a_1^2 - 4a_0}) \tag{4.4}$$

The transfer functions of the orthogonal modes in x and y are complex, so the eigenvalue is complex as well.

$$\Lambda = \Lambda_R + i\Lambda_I \tag{4.5}$$

The expression for chatter-free axial depth of cut is given as :

$$a_{lim} = -\frac{2\pi\Lambda_R}{NK_t}(1 + \kappa^2) \tag{4.6}$$

where $\kappa = \frac{\Lambda_I}{\Lambda_R}$. K_t is the tangential cutting coefficient and N the number of teeth.

The spindle speed is obtained by finding the corresponding tooth passing frequency :

$$T_f = \frac{1}{\omega_c}(\varepsilon + 2k\pi) \quad k=0,1,2,... \tag{4.7}$$

and then the spindle speed n [rev/min] :

$$n = \frac{60}{NT_f}. \tag{4.8}$$

By looking at the equation for a_{lim}, it is apparent that stability lobes are function of the transfer functions of the system, the width of cut (through the directional dynamic milling coeffi-

cients), the number of teeth N and the cutting coefficient K_t, which correspond respectively to the dynamic parameters of the tool-machine system, the cutting geometry, the cuting tool geometry and the workpiece material.

Stability lobes are presented as a graph that relates the axial depth of cut to the spindle speed. Figure 4.2 shows an example of stability lobes. The region under the curve is the stable region while cutting conditions above the curve correspond to chatter conditions.

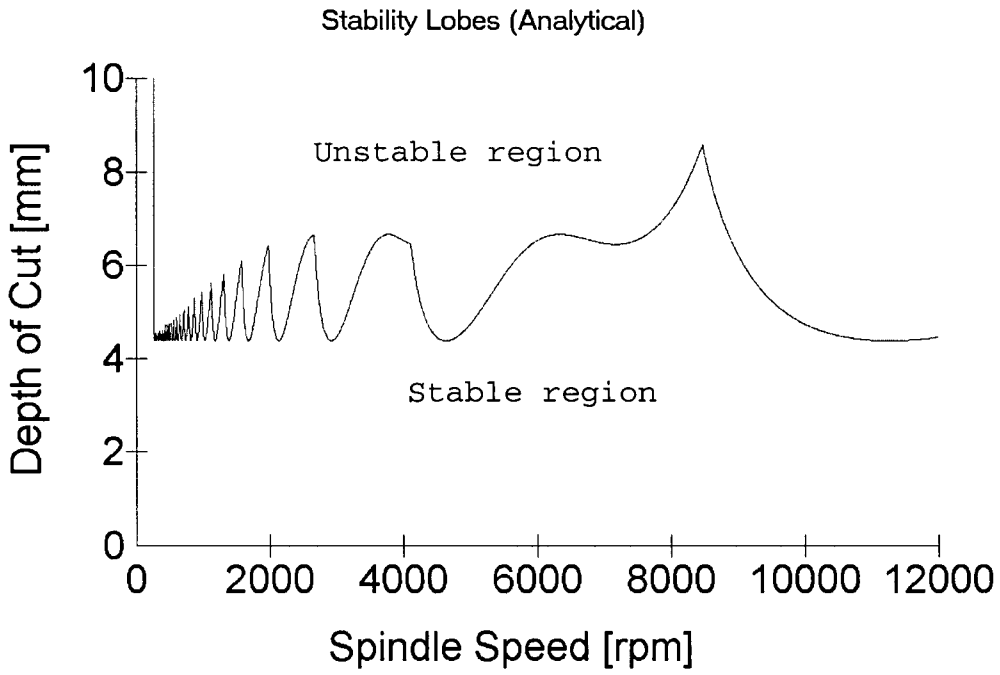

Figure 4.2 : Example of stability lobes.

4.3.2. Flowchart for the Selection of Stable Cutting Conditions

As mentioned in the previous section, calculation of stability lobes requires that some elements of the cutting process be specified by the user. The following parameters and cutting conditions are selected or entered via the interface: workpiece material, selection of the cutting tool, tool and workpiece frequency response functions, and the radial depth of cut. The interface must be integrated in the CAD/CAM software and must allow for the selection of all the parameters and cutting conditions previously mentioned. The flowchart presented in figure 4.3 illustrates the steps that the user follows in the selection/entry of these parameters. The boxes on the right side correspond to tasks performed by the application according to the selections made by the user.

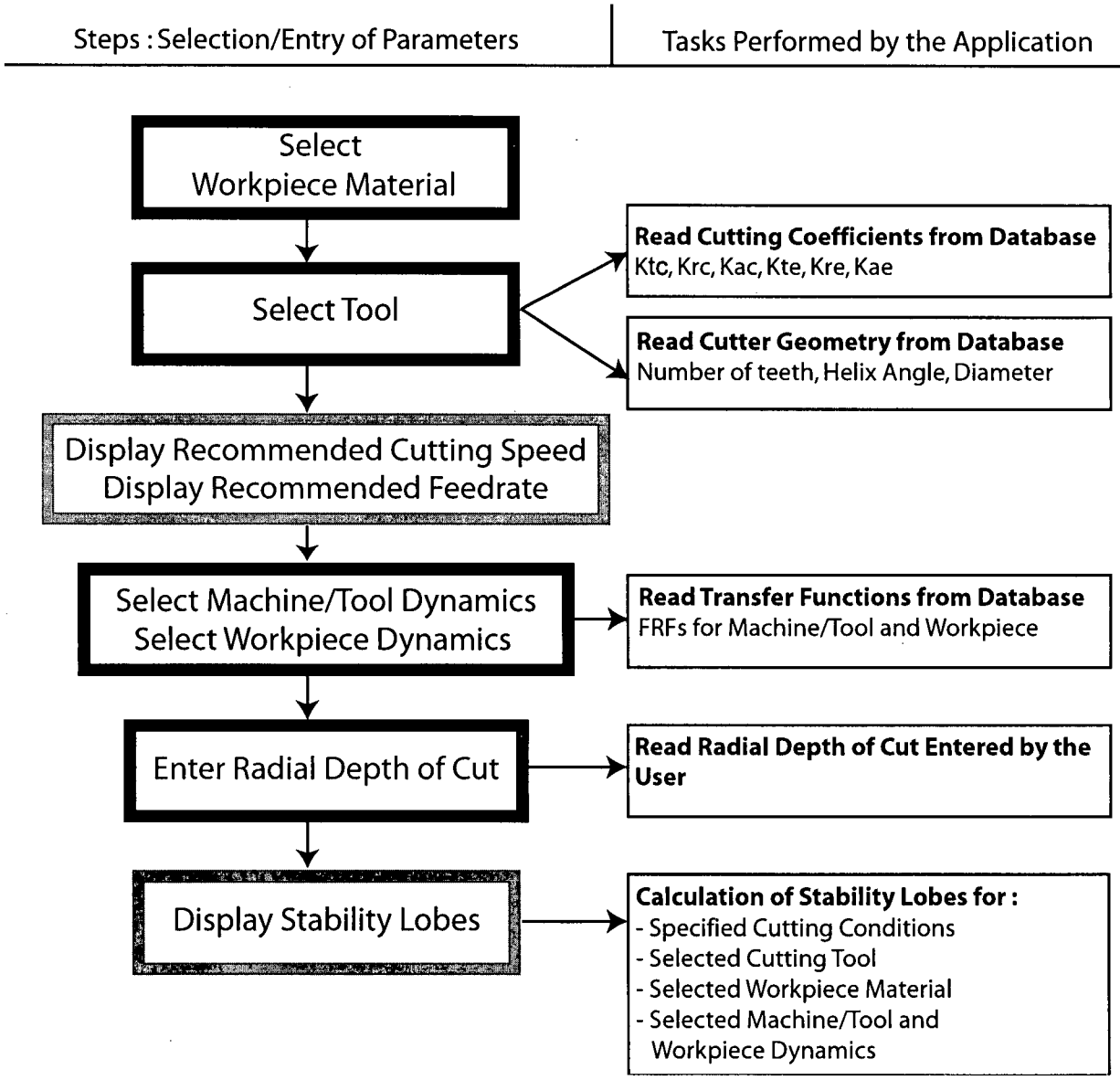

Figure 4.3 : Flowchart - Interface in CAD/CAM software for the selection of cutting conditions.

The first step is the selection of workpiece material in a list of materials available. Once the material is selected, a list of tools for which mechanistic cutting tests have been performed is shown.

The second step is the selection of the appropriate cutting tool for the operation. With the workpiece material and cutting tool selected, the associated milling cutting force coefficients are extracted from the database. Recommended cutting speed and feedrate range are then displayed. The user uses this information as a reference to program the feedrate.

The third step is the selection of the machine/tool and workpiece dynamics. The frequency response function of the cutting tool is necessary to calculate the stability lobes, while the frequency response function of the workpiece is selected only for the case of a flexible workpiece.

The fourth step is the entry of the radial depth of cut used in the operation.

With all the information extracted from the database and entered by the user, the stability lobes are calculated and displayed to the user in order to select appropriate spindle speed and axial depth of cut for the operation.

4.3.3. Development of an Interface in CATIA

Following the flowchart presented above, an interface is developed using Visual Basic programming language. This interface is integrated in the Prismatic Machining module of the software CATIA V5. The interface is divided in two windows. The main window is shown in figure 4.4. In this window, the user specifies information regarding the process, i.e. workpiece material, cutting tool selection, cutting tool and workpiece frequency response functions and width of cut. The second window is shown in figure 4.5. It is used to display the stability lobes for the cutting parameters and the selections previously made.

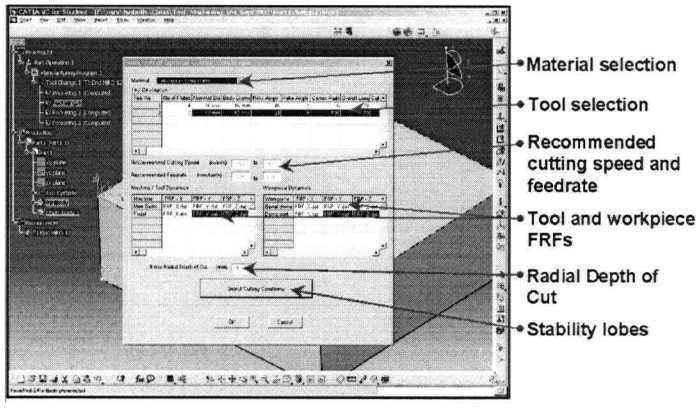

Figure 4.4 : CATIA interface : selection of cutting conditions.

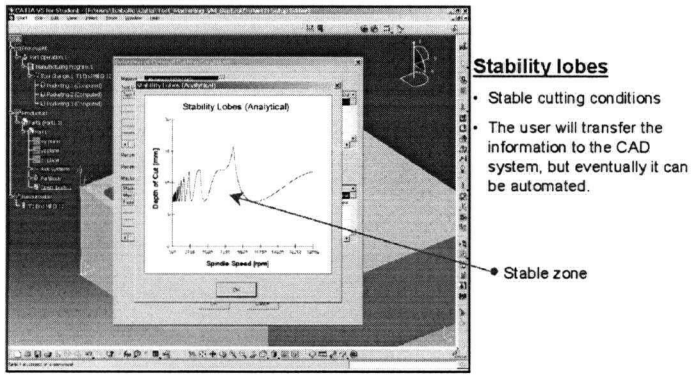

Figure 4.5 : CATIA interface: stability lobes.

Using the stability lobes, the NC programmer selects a set of spindle speed and depth of cut under the curve in order to avoid chatter conditions.

4.4. Workpiece Model and NC Tool Path

The geometry of the blank and final part are created in the CAD/CAM software. In order to be read by the application in ACIS for the cutting tool - workpiece intersection calculations, they

are converted to the STEP format. The NC tool path is programmed in the CAD/CAM software. The corresponding APT file is generated and transferred to the application in ACIS.

Using STEP files for the part geometry and APT file for the NC toolpath means that any commercial package capable of converting to these formats can be used, therefore it is independent of the CAD/CAM software.

4.5. Cutting Tool - Workpiece Intersection

In order to simulate the milling operation, the virtual milling application requires input regarding the process. To calculate the cutting forces as well as the torque and power, and tool deflection, it is necessary to know for each step along the tool path the following parameters: the entry and exit angles which define the radial width of cut, the feedrate, the spindle speed and the axial depth of cut.

The application developed in ACIS by Huang [25] to calculate the intersection between the tool and the workpiece reads the APT file generated by the CAD/CAM software. This file contains APT instructions describing the motions of the tool programmed. It is necessary to discretize the tool path in order to catch the geometry changes. Therefore, the current version of the application calculates the intersection along the tool path at small intevals, such as 0.5, 1 or 2 mm, or as specified by the user. A later version of the application will recognize automatically areas where it is necessary to discretize the tool path and other areas where it is not. This improvement will reduce greatly the computation time.

Another information required is the angle between the tool path and the machine X axis. The cutting forces are measured in the X, Y and Z directions. The entry and exit angles are given according to the local coordinate system for a specific location on the tool path. The cutting forces are calculated in this system and they are projected on X and Y, as seen in section 3.8.2.

4.5.1. Structure of the Tool-Workpiece Intersection Output File

The application in ACIS generates an output file which is read by the milling process simulation. This output file has the following format :

1 : number of pairs of entry-exit angle;

2 : sets of entry-exit angles [radians];

3 : X, Y and Z coordinates [mm];

4 : angle between local coordinate system and X-Y machine system [radians];

5 : depth of cut [mm];

6 : spindle speed [rpm];

7 : feedrate [mm/min].

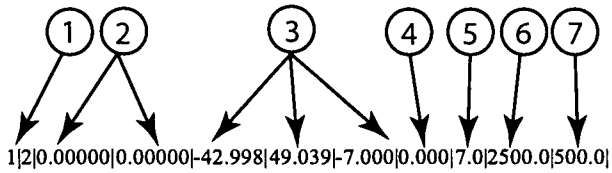


```
1|2|0.00000|0.00000|-42.998|49.039|-7.000|0.000|7.0|2500.0|500.0|
0|-40.998|49.039|-7.000|0.000|
1|2|1.55241|1.58918|-9.998|49.039|-7.000|0.000|7.0|2500.0|500.0|
1|2|0.92701|2.21458|-7.998|49.039|-7.000|0.000|7.0|2500.0|500.0|
1|4|0.00000|1.13028|1.36782|3.14159|1.002|49.039|-7.000|0.000|7.0|2500.0|500.0|
```

Figure 4.6 : Example of tool-workpiece intersection output file.

4.6. Milling Process Simulation

The milling process simulation application can be divided into two components. The first component is the engine that calculates the instantaneous cutting forces, maximum forces, maximum torque and power, as well as deflection and maximum deflection. The second component is used to perform feedrate scheduling. Functions from the milling process simulation application are called to calculate maximum force, maximum torque and power, maximum deflection, in order to schedule the feedrate according to these constraints. The output of the milling process simulation is an optimized CL file.

4.6.1. Data Structure

The milling process simulation is programmed in C++. The main class provides methods to calculate forces, torque and power, deflection, and perform feedrate scheduling. For each step along the tool path, information is read from the tool-workpiece intersection output file and results are stored. Figure 4.7 shows the structure used to store this information.

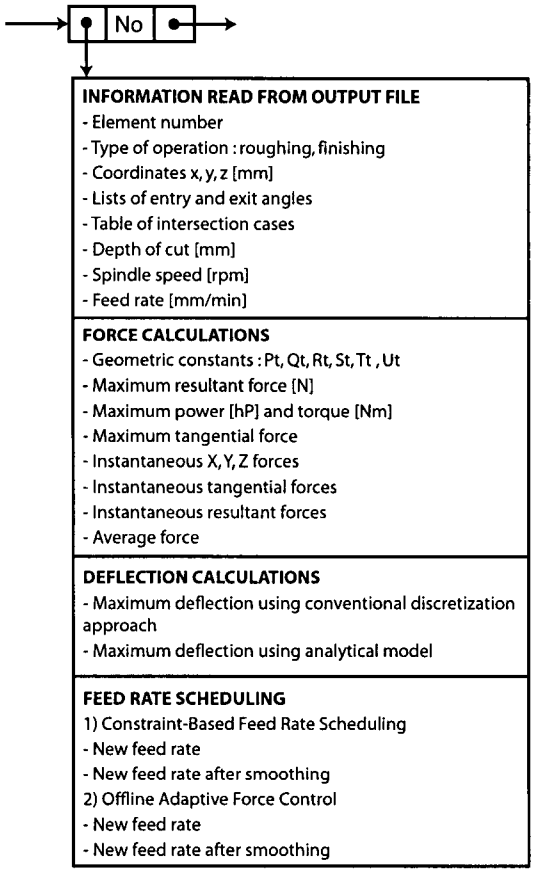

Figure 4.7 : Milling process simulation - Data structure for each step.

4.7. Feedrate Scheduling

Optimization of the machining tool path can be performed either off-line or on-line during the machining operations. On-line monitoring of the forces, etc... in order to modify the spindle speed and feedrate, requires the use of additional measuring equipment and modifications to the machine tool and its controller. It is usually used once to optimize the parameters and register the new NC program. Off-line methods are based on models which try to represent as accurately as

possible the physics of the process. More cutting conditions can be modified using off-line approach, as with the on-line method it is rather difficult to modify the tool path itself, while with off-line it is always possible to modify the depths of cut, etc...

In this research project, we are going to compare 3 approaches, two off-line approaches and one on-line approach. In all cases, only the feedrate can be adjusted. Since there is no existing link between a milling simulation system and a commercial CAD/CAM software, it would be rather difficult to modify the cutting geometry, i.e. the axial and radial depths of cut. Our application provides options that are readily usable in a commercial setting. Therefore, only the feedrate can be adjusted.

The 2 off-line methods are constraint-based feedrate scheduling and off-line adaptive force control. On-line approach is done using an application programmed and available in the Manufacturing Automation Laboratory [3].

During the machining operation, sudden changes in the workpiece geometry may result in increase in the depth of cut or immersion. These changes might cause force overshoots, creating situations where the forces and stresses exerted on the cutting tool may exceed the tool capacity as well as exceed the spindle motor power. These situations are potential risk of severe damage to the tool and machine and should be avoided. Other objectives of feedrate scheduling is to reduce the machining cycle time and improve the workpiece surface finish and accuracy.

In the following sections, we will explain all three approaches and complete this part with the approach used to smooth the new optimized feed curve.

4.7.1. Constraint-Based Feedrate Scheduling

Roughing and finishing operations do not have the same requirements. During roughing, the objective is to achieve the highest material removal rate, as it is economical to reduce the machining time as much as possible, while the objective in finishing is to meet close part tolerances and achieve good surface finish. For feedrate scheduling, the following constraints will be considered: maximum force, maximum torque and power, maximum chip load and maximum deflection.

Roughing

In roughing, large forces and tool deflections are allowed as the focus is on the volume of material removed. The maximum force, maximum torque and power, and maximum chip load will be checked.

The loads on the cutting tool will be high considering aggressive cutting conditions are selected to machine the part as quickly as possible. It is important to verify that the maximum cutting force will not be exceeded, which could result in tool shank breakage, and to adjust the feedrate accordingly.

The machine tool and its spindle motor are designed for certain types of machining applications. Spindle motors specifications are defined in a chart of the maximum torque and power available versus the spindle speed. Maximum torque and power need to calculated in order to assure that the cutting conditions will not overload the machine spindle, causing important damage and possible failure of this component.

The cutting tool edges are submitted to large stress and the allowable tooth stress is expressed by the tool manufacturer in the form of chip load. Therefore, we need to check that the chip load is not exceeded.

Finishing

In finishing, deflections should be minimized and we want to achieve close tolerances and meet the surface finish requirement. The same constraints as for roughing will be considered, as well as the maximum deflection constraint.

Maximum Force

The maximum force constraint $F_{RES,max}$ is evaluated in order to avoid shank breakage. As stated earlier in equations 3.13 and 3.14, the forces in X and Y are given by :

$$F_{x,ij}(\phi) = \frac{1}{k_\psi}\left[K_{TE}S_{ij} - K_{RE}U_{ij} + \frac{s_{t,force}}{4}[K_{RC}T_{ij} - K_{TC}R_{ij}]\right]\Bigg|_{z_{ij1}}^{z_{ij2}}$$

$$F_{y,ij}(\phi) = \left(-\frac{1}{k_\psi}\right)\left[-K_{TE}U_{ij} - K_{RE}S_{ij} + \frac{s_{t,force}}{4}[K_{TC}T_{ij} - K_{RC}R_{ij}]\right]\Bigg|_{z_{ij1}}^{z_{ij2}}$$

The resultant force in the X-Y plane is given by :

$$F_{RES,max} = \sqrt{F_x^{\,2} + F_y^{\,2}}$$

We can define F_x and F_y as :

$$F_x = A + s_{t,force}B \tag{4.9}$$

$$F_y = C + s_{t,force}D \tag{4.10}$$

where the variables A, B, C and D, are :

$$A = \frac{1}{k_\psi}(K_{TE}S_T - K_{RE}U_T)$$

$$B = \frac{1}{4k_\psi}(K_{RC}T_T - K_{TC}R_T)$$

$$C = \left(-\frac{1}{k_\psi}\right)(-K_{RE}S_T - K_{TE}U_T)$$

$$D = \left(-\frac{1}{4k_\psi}\right)(K_{TC}T_T + K_{RC}R_T)$$

The cutting coefficients K_{TC}, K_{TE}, K_{RC} and K_{RE} are known for a given position of the tool as well as the geometric constants. F_{RES} is the maximum allowable force on the tool. The feed per tooth $s_{t,force}$ is the unknown.

The resultant force $F_{RES,max}$ takes the form :

$$F_{RES,\,max} = \sqrt{(A + s_{t,force}B)^2 + (C + s_{t,force}D)^2}$$

The following quadratic equation is obtained :

$$s_{t,force}{}^2(B^2 + D^2) + s_{t,force}(2AB + 2CD) + A^2 + C^2 - F^2{}_{RES,\,max} = 0 \qquad (4.11)$$

and in a simplified form :

$$Js_{t,force}{}^2 + Ks_{t,force} + L = 0$$

where J, K and L are :

$$J = B^2 + D^2$$

$$K = 2AB + 2CD$$

$$L = A^2 + C^2 - F_{RES,\,max}{}^2$$

The feed per tooth is obtained by solving for $s_{t,force}$, the unknown.

$$s_{t,force} = \frac{-K \pm \sqrt{K^2 - 4JL}}{2J} \tag{4.12}$$

We only consider the positive values of $s_{t,force}$ and keep the lowest value.

Maximum Torque and Power

It is important to verify that the torque and power requirements do not exceed the machine spindle capacity and to adjust the feedrate accordingly to use the maximum torque and power available at a given spindle speed.

The maximum torque and power were given by equations 3.20 and 3.24 :

$$T_{max} = F_{t,\,max} \times r_c$$

$$P_{max} = (T_{max} \cdot n)[kW]$$

The maximum torque and power are function of the spindle speed. Typically, the machine tool builder provides a torque/power chart. As an example of this type of chart, the chart for the horizontal milling machine Mori Seiki SH-403 is presented in figure 4.8.

If we do not consider its direction, the tangential force F_t is given :

$$F_{t,\,max} = K_{TE} Z_T - \frac{K_{TC} s_{t,\,torque}}{k_\psi} U_T$$

The torque is :

$$T_{max} = \left(K_{TE} Z_T - \frac{K_{TC} s_{t,\,torque}}{k_\psi} U_T\right) \frac{r_c}{1000} \tag{4.13}$$

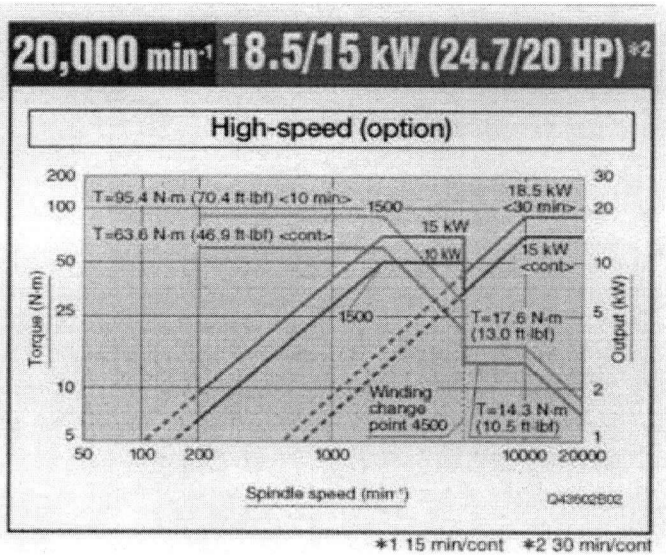

Figure 4.8 : Torque and power chart - Mori Seiki SH-403.
Source : Mori Seiki Company.

The feed per tooth $s_{t,torque}$ is :

$$s_{t,\,torque} = \left(\frac{T_{max} \cdot 1000}{r_c} - K_{TE} Z_T\right) \frac{k_\psi}{K_{TC} U_T}. \tag{4.14}$$

Maximum Chip Load

The maximum chip load corresponds to the maximum recommended chip load by the tool manufacturer or found in handbooks. The maximum chip load is found with :

$$h_{max} = s_{t,\,chip} \sin \phi_j$$

Calculations are done for the values of ϕ_{st} and ϕ_{ex} for each set of entry-exit angles. If $\pi/2$ is part of one of the intervals, then the maximum chip load will occur at this angle and is equal to the feed per tooth since sin $\pi/2$ is equal to 1.

$$s_{t,\,chip} = \begin{cases} s_{t,\,chip} = h_{max} & \text{if } \frac{\pi}{2} \in [\phi_{sti}, \phi_{exi}] \\ s_{t,\,chip} = min\langle h_{max}/(\sin\phi) | (\phi = \phi_{st,\,0}, \phi_{ex,\,0}, \phi_{st,\,1}, \ldots)\rangle \end{cases} \quad (4.15)$$

Maximum Deflection

The maximum deflection is calculated using the model presented in section 3.7.2. The constraint is set as the tolerance allowable for the part. The maximum deflection was given in equation 3.31 :

$$\delta_{y,\,max} = \frac{F_{y,\,max} A^2 (A - 3L)}{6EI}$$

The constants A, E, I and L depend on the geometry of the cut and the tool material. We set $\delta_{y,\,max}$, so we can find $s_{t,def}$. $F_{y,max}$ can be expressed as earlier as :

$$F_{y,max} = C + s_{t,\,def} D$$

where

$$C = \left(-\frac{1}{k_\psi}\right)(-K_{RE} S_T - K_{TE} U_T)$$

$$D = \left(-\frac{1}{4k_\psi}\right)(K_{TC} T_T + K_{RC} R_T).$$

So, the feed per tooth $s_{t,def}$ becomes :

$$s_{t,\,def} = \frac{\left(\frac{\delta_{max} 6EI}{A^2(A - 3L)}\right) - C}{D} \quad (4.16)$$

Identification of maximum allowable feedrate

The maximum allowable feedrate is the minimum of all feedrates calculated :

$$s_{t,\,opt} = min(s_{t,\,force},\, s_{t,\,torque},\, s_{t,\,power},\, s_{t,\,chip},\, s_{t,\,def}) \tag{4.17}$$

The new feedrate commands might not produce a smooth feedrate curve. In order to get a smoother curve, we use a 5-point average smoothing method where the 4 previous feed values ($s_{t,k-4}$, $s_{t,k-3}$, $s_{t,k-2}$, $s_{t,k-1}$) and the current feed $s_{t,k}$ are used, and the average over these 5 points is calculated to obtain the new feed for step k.

$$s_{t,\,k,\,new} = \frac{s_{t,\,k-4} + s_{t,\,k-3} + s_{t,\,k-2} + s_{t,\,k-1} + s_{t,\,k}}{5} \tag{4.18}$$

The NC program is then updated with new F commands for each step.

4.7.2. Adaptive Force Control

When machining, the quality of the workpiece and the performance of the machine are related largely to the CNC feed drive dynamics and the cutting process dynamics. Using adaptive control in machining provides improved machining parameters by adapting to the changes in the cutting operation, such as depth of cut and width of cut.

In this research project, both approaches, off-line and online adaptive force control, are based on the adaptive generalized predictive control developed by Altintas [9] and are used to maintain the peak force at a specified reference cutting force by updating the feedrate command. This

adaptive control algorithm is based on Generalized Predictive Control method presented by Clarke et al[20].

The block diagram presented in figure 4.9 shows the general adaptive control system. In this block diagram, we can see that the input to the milling process is the feed command f_c while the output is the resultant cutting force F_a applied at the tool tip.

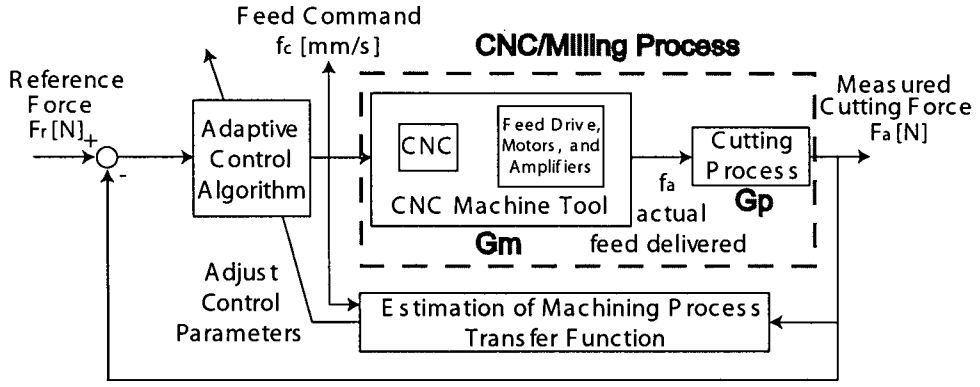

Figure 4.9 : Block diagram of a general adaptive control system in machining.
Source : Altintas [9].

The CNC and feed drive dynamics can be modelled as [6]:

$$G_m(z) = \frac{f_a(z)}{f_c(z)} = \frac{(g_0 + g_1 z^{-1} + g_2 z^{-2})}{1 - h_1 z^{-1}} \tag{4.19}$$

where f_c is the feed command to the CNC and f_a is the actual feed delivered by the drives. The parameters g_0, g_1, g_2 and h_1 vary with the feedrate and spindle speed.

The milling process can be expressed by the transfer function [6]:

$$G_p(z) = \frac{F_a(z)}{f_a(z)} = \frac{\beta z^{-1}}{1 + \alpha z^{-1}} \tag{4.20}$$

where

$$\mu = \frac{K_s a}{k_t}, \alpha = \frac{-\mu}{1+\mu}, \beta = \frac{k_t \mu}{Mn(1+\mu)}.$$

where M is the number of teeth, n is the spindle speed [rps], K_s is the cutting coefficient and k_t is the stiffness of the tool.

Therefore, the transfer function of the plant is given by [9]:

$$G_c(z) = G_m \times G_p = \frac{F_a(z)}{f_c(z)} = \frac{B(z)}{A(z)} = \frac{z^{-1}(b_0 + b_1 z^{-1} + b_2 z^{-2})}{1 + a_1 z^{-1} + a_2 z^{-2}} \tag{4.21}$$

where $b_0 = g_0 \times \beta$, $b_1 = g_1 \times \beta$, $b_2 = g_2 \times \beta$, $a_1 = -h_1 + \alpha$ and $a_2 = -h_1 \times \alpha$.

The plant dynamic parameters can be estimated using a Recursive Least Square (RLS) algorithm [9].

Online Adaptive Force Control

For the online approach, the X and Y forces are measured during the machining using a dynamometer and transferred to the adaptive controller which adapts the parameters and generates a new feedrate command. The new feedrate command is sent to the CNC and the new resultant force is measured.

Off-line Adaptive Force Control

The adaptive generalized predictive control developed by Altintas [9] was also implemented in the Virtual Milling project. The difference with the online adaptive control is that in this case, the resultant cutting force is not measured during the machining but calculated by the milling simulation.

4.8. Simulation and Experimental Results

4.8.1. Set-up

Experimental cutting tests were performed on a Fadal vertical machining center equipped with both a Kistler dynamometer and the Open Architecture Real-Time Operating System (ORTS). ORTS is a general purpose real-time operating system running on a DSP board connected to a PC. This system was developed in the Manufacturing Automation Laboratory at the University of British Columbia [4]. The cutting forces in X and Y are measured using the Kistler dynamometer. For the cutting tests for constraint-based feedrate scheduling and offline adaptive force control, the cutting forces are recorded using the MAL-DAQ module from CutPro [10]. For the online adaptive force control, the cutting forces are fed into the interface board of ORTS. For all three approaches, NC programs were transferred to the machine tool controller.

For constraint-based feedrate scheduling and offline adaptive force control, simulations using the milling simulation module and the corresponding feedrate scheduling algorithm are first run. Feedrate curves and modified NC programs are obtained.

For online adaptive force control, the original NC program is fed to the controller and the adaptive force control algorithm implemented in ORTS adjusts the feedrate according to the cutting forces and controller parameters. ORTS is connected directly to the controller's feed override potentiometer.

4.8.2. Tests

The tests were performed for the milling operation shown in figure 4.10. The three pockets were previously machined at a depth of cut of 8 mm and the test consists in the linear tool path shown by the segment from point A to B. The axial depth of cut is 2 mm. The dimensions of the workpiece and its features are given in figure 4.11.

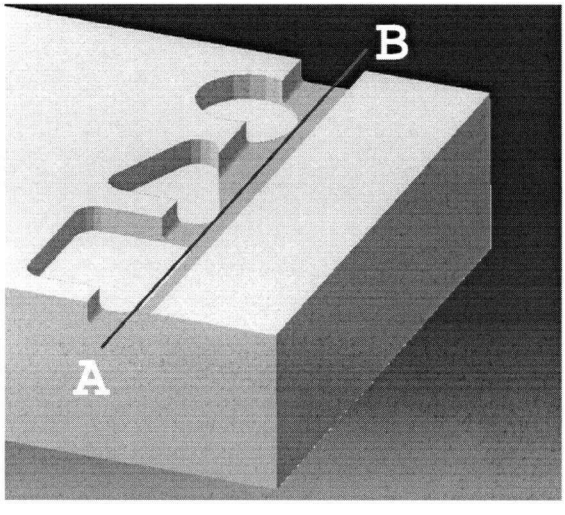

Figure 4.10 : Test part - Toolpath.

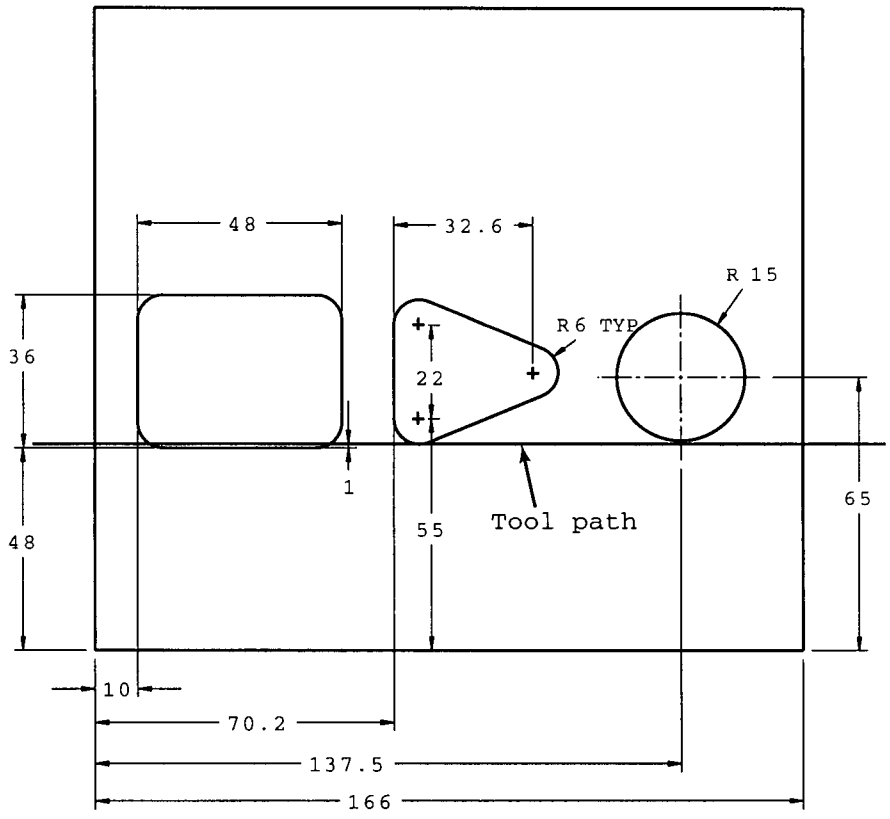

Figure 4.11 : Test part - Dimensions.

The workpiece material is Al7075-T7451. The cutting tool is a two-flute cylindrical end mill with a diameter of 12mm, a rake angle of 8 degrees and a helix angle of 30 degrees. The spindle speed used is 2500 rpm and the depth of cut is 2 mm. The parameters used for the tests were as follows : the maximum allowable feedrate is set to 2000 mm/min and the reference cutting force is 350 N.

Simulation Results

First, simulations using constraint-based feedrate scheduling and off-line adaptive force control are conducted to obtain feed curves that are used for the experimental milling tests. The feed curves are shown in figures 4.12 and 4.13. These curves show the feedrate as a function of the position of tool along the toolpath. Figure 4.14 shows the corresponding simulation results for the resultant peak force. We choose to display these curves using position instead of time as position refers directly to the NC code that is generated and sent to the machine tool controller.

From these curves, we can observe some differences. At position 35 mm, both algorithms detect a force increase as the cutting tool enters the workpiece. The constraint-based approach decreases the feedrate faster and in the simulation results, it reaches the desired reference cutting force at 40 mm. Both approaches give similar feedrates for the segment of the tool path where the tool machines the side of the rectangular feature. At position 80 mm, the algorithms detect again a change in the geometry as the cutting tool enters the section between the rectangular and triangular features. Again, constraint-based approach brings the simulation force back to the reference value faster than the offline adaptive force control. As the tool is going through the triangular feature, both algorithms increase the feedrate in a similar manner with a very similar peak feedrate at position 120 mm. As the cutting tool is going through the last circular feature, we observe a smooth peak with the offline adaptive force control.

The simulation results for peak forces using those feed curves gave good results with slight deviations from the reference cutting force of 350 N.

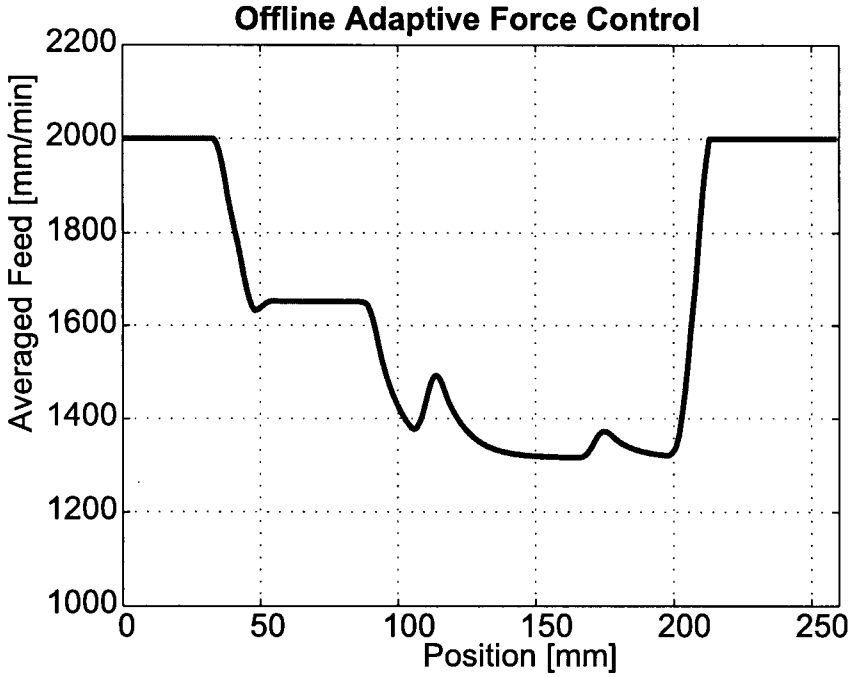

Figure 4.12 : Feed curve - Offline adaptive force control.

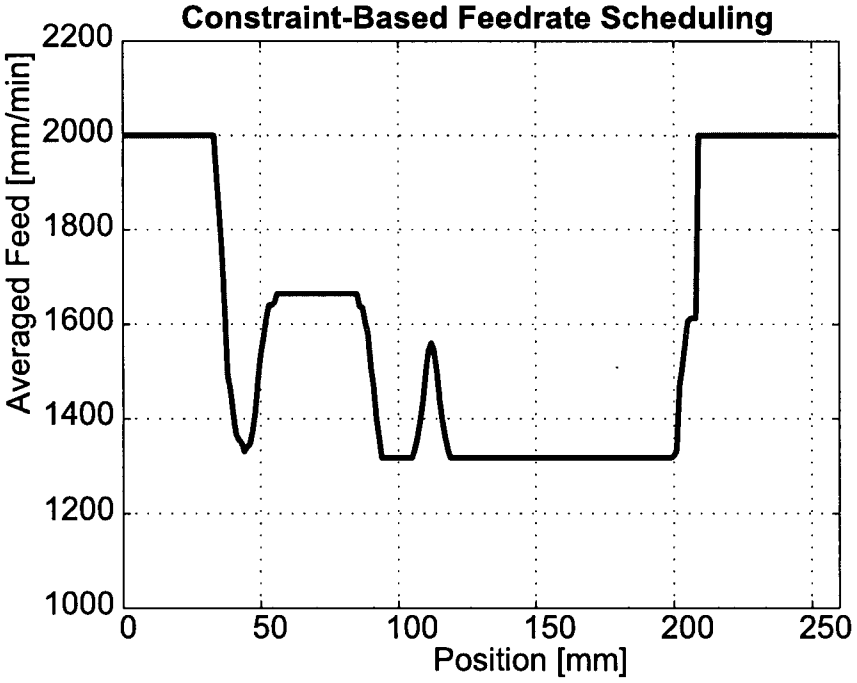

Figure 4.13 : Feed curve - Constraint-based feedrate scheduling.

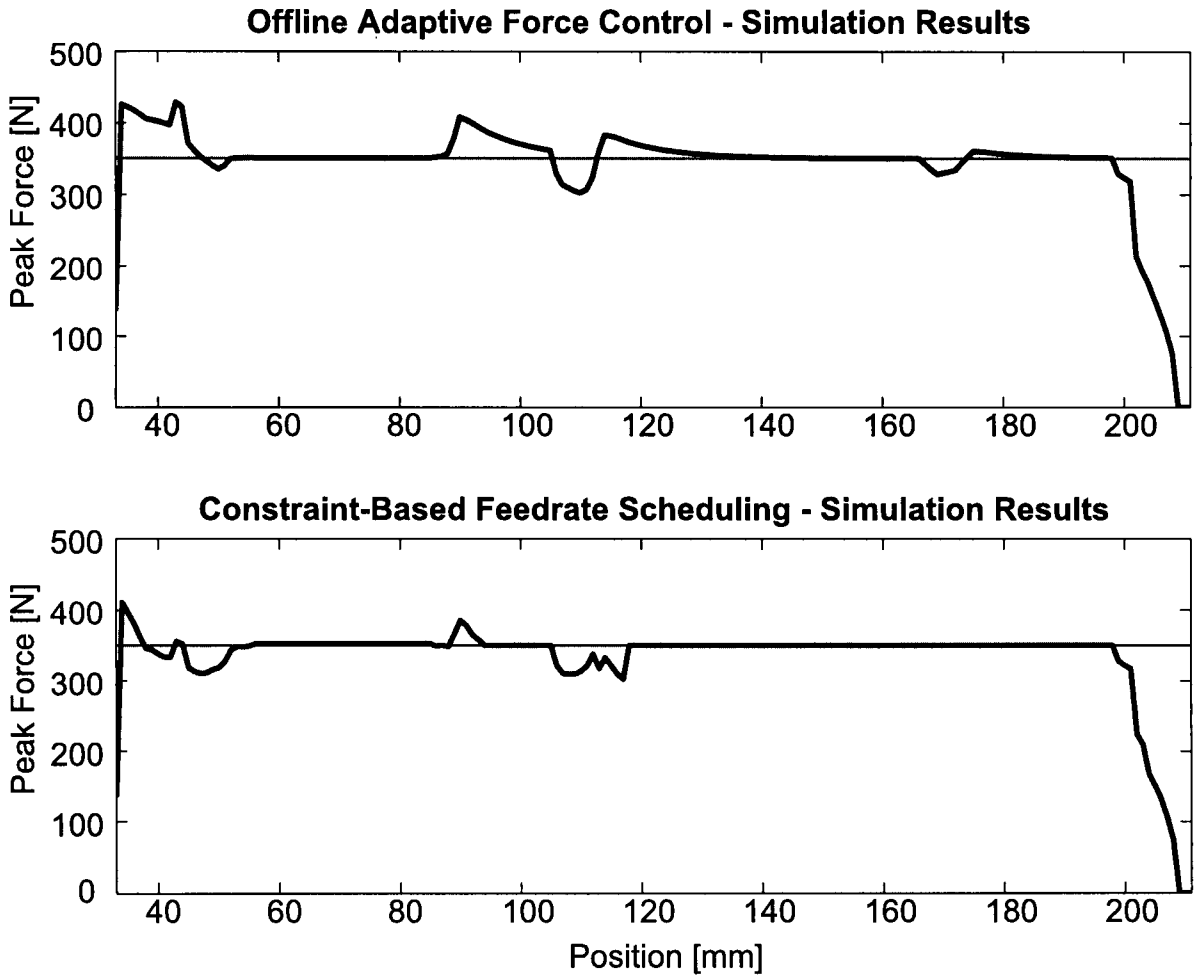

Figure 4.14 : Simulation of peak forces.

Experimental Results

Experiments are conducted for the 3 approaches. For the constraint-based approach and the off-line adaptive force control approach, the NC programs are defined using the feed curves obtained by simulation. For online adaptive force control, a NC program is first fed to the

machine controller and the ORTS and the adaptive control algorithm adjusts the feedrate in order to meet the process specifications, that is the reference force and maximum feedrate.

Figure 4.15 shows the feed curve obtained when using online adaptive force control. The feedrate is given as a function of time, but we can observe a similar trend as for the simulation feed curves obtained with the off-line approaches.

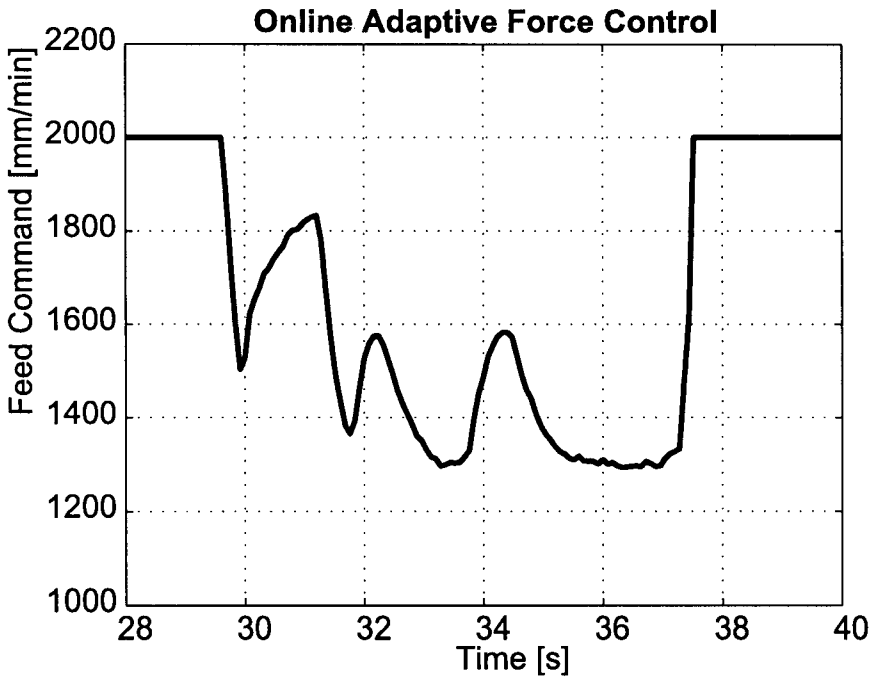

Figure 4.15 : Feed curve - Online adaptive force control.

The experimental results for the peak force measurements are presented in figure 4.16. As we can see, all three approaches give good results. For all three approaches, there is an overshoot when the cutting tool enters the workpiece and between features. The overshoot is about 20% for the online adaptive force control as the tool enters the workpiece, which is slightly higher than with the off-line approaches. Also, between the rectangular pocket and the triangular pocket, the

online adaptive force control gives a higher overshoot. On the other hand, this approach gives a smoother peak force curve than the other approaches.

In terms of cycle time, the online adaptive force control is the method that gave the best results with a time of 8 s. For off-line adaptive force control, the cycle time was 9 s and for constraint-based feedrate scheduling it was 9.9 s.

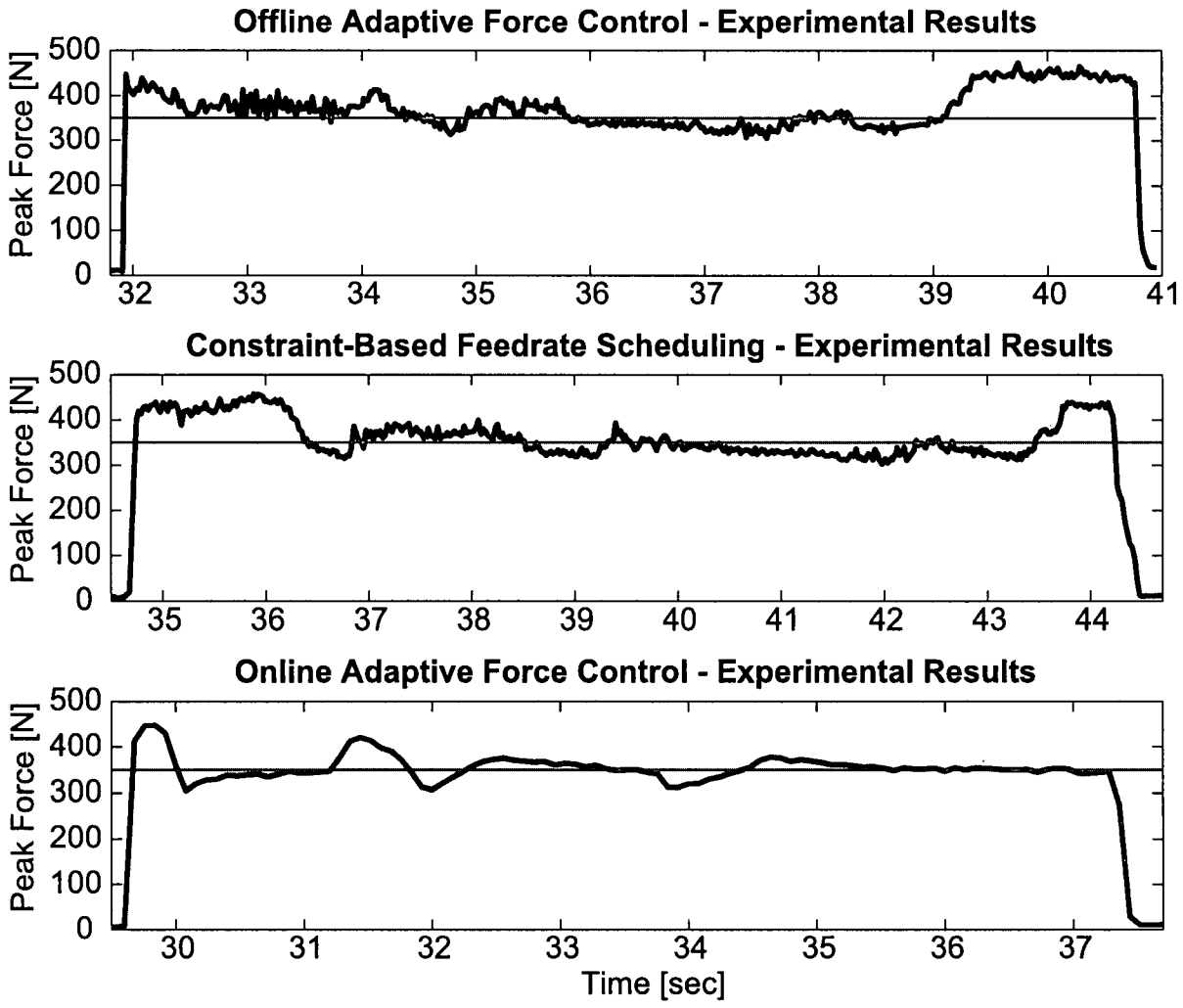

Figure 4.16 : Experimental peak forces.

4.9. Conclusion

Based on the analytical milling force model developed by Spence [36] and presented in chapter 3, a framework for the implementation of Virtual Milling was developed. This application comprises a new interface for the selection of stable cutting conditions. This interface is integrated in a CAD/CAM software, which is new since current CAD/CAM systems do not offer such options. This is the first step in the Virtual Milling project. This interface was developed and integrating in the milling module of CATIA V5.

The validation of the force model was presented in the previous chapter. Two approaches for feedrate scheduling, constraint-based feedrate scheduling and off-line adaptive force control, were implemented. These 2 approaches were tested and compared with a third approach, online adaptive force control. Cutting tests were done and all three approaches prove to give good results. On-line adaptive force control seems to be the most efficient approach since it gives good results for peak force and the lowest cycle time, but it requires testing on the machine. The two off-line approaches are an interesting alternative and even though they did not perform as well as the online adaptive force control, they provide an improvement in terms of force control and cycle time compared to traditional NC programming practices.

Conclusion

Milling process simulation is becoming part of engineering practices in advanced manufacturing facilities. The next step is to integrate the milling process simulation and the CAD/CAM capabilities to simulate the machining operation for the whole NC program. This is known as Virtual Milling and offers many advantages such as the capability to identify critical cutting conditions, to calculate cutting forces and deflections along the tool path in order to improve part quality and meet part tolerances, to reduce the machining cycle time by performing feedrate scheduling, and to reduce or eliminate the tool proofing time before production start. This thesis presents an application for Virtual Milling developed and tested for 2 1/2 D parts.

The first section of this work, the milling simulation, involved modelling of the milling process for the whole part and was done by implementing the analytical closed-loop form milling force model developed by Spence [36]. This analytical model has the advantage of requiring less computation time since integration along the tool axis is not required. The input is a file generated by the tool-workpiece intersection application developed in ACIS by Huang [25]. This file contains the tool-workpiece intersections along the discretized tool path. The output of the milling simulation include instantaneous forces, resultant forces, maximum forces, maximum torque and power, deflections along the tool axis and maximum deflection, for each step along the tool path. In order to validate the model, experimental cutting tests were performed on a 2 1/2 D part. The test part featured different geometries and different intersection cases. Experimental results were compared with simulation results and showed that the milling force model is relatively accu-

rate, with an error of about 10%. The principal source of error is the modelling of the material cutting coefficients.

Then, the Virtual Milling flowchart was presented. The first step in Virtual Milling is the selection of appropriate and stable cutting conditions during the NC programming. Once the NC program is completed, it is more difficult to modify the axial depth of cut as it requires to modify the tool path itself. If the user is guided in the selection of the axial depth of cut that will provide stable cutting, the NC program will not require subsequent modifications. Current CAD/CAM systems do not offer tools for the selection of cutting conditions. Therefore, the requirements of such a tool were estalished and a new interface was developed and integrated in the Prismatic Machining module of the CAD/CAM software CATIA V5. This interface provides the user with a chart of the axial depth of cut as a function of the spindle speed, known as stability lobes. The user must first select the cutting tool geometry and workpiece material in a database, then select the tool-machine transfer functions, and specify the radial width of cut used in the program. These input are necessary for the calculation of stability lobes. The NC programmer can then select a proper combination of axial depth of cut and spindle speed using the stability lobes.

The second step in the Virtual Milling is the milling simulation. The milling simulation is used for two purposes : to evaluate the milling operation and check its validity, and to perform feedrate scheduling. The first purpose allows the user to identify problematic sections of the tool path. The second use for milling simulation is to perform feedrate scheduling. Two off-line approaches were implemented: constraint-based feedrate scheduling and off-line adaptive force control. These approaches were used to generate feed curves for a specific tool path in order to evaluate the gain from using off-line approaches. Experimental cutting tests were conducted.

Another approach, online adaptive force control developed by Altintas [9] was also used during the tests in order to compare the three methods. All three methods gave good results. There were overshoots at transient cuts in all cases, the maximum overshoot of about 20% was observed with the online adaptive force control. On the other hand, the machining time was lower with this approach and the constraint-based feedrate scheduling was the slowest method. Overall, the off-line approaches can be used to adapt the feedrate to specific machining constraints and will provide good control of the cutting forces while improving the machining time.

Future Research

This thesis focused on Virtual Milling for 2 1/2 D parts using cylindrical end mills. Future work should include complex geometries, such as sculptured surfaces and 5-axis machining, as well as different tool geometries.

The milling simulation should provide the user with information regarding locations of critical constraints along the tool path. Ideally, it should be integrated in the CAD/CAM software and could run in real-time with the visualisation of the metal removal.

Bibliography

[1] Altintas Y., Yellowley I., Tlusty J., 1988, *The Detection of Tool Breakage in Milling Operations*, ASME Journal of Engineering for Industry, Vol.110, pp.271-277.

[2] Altintas Y., Spence A.D., 1991, *End Milling Force Algorithms for CAD Systems*, Annals of the CIRP, Vol.40 (1), pp.31-34.

[3] Altintas Y., 1994, *Direct Adaptive Control of End Milling Process*, International Journal of Machine Tools and Manufacturing, Vol.34, No.4, pp.461-472.

[4] Altintas, Y., Munasinghe W.K., 1994, *A Hierarchical Open-Architecture CNC System for Machine Tools*, Annals of the CIRP, Vol.43/1, pp.349-354.

[5] Altintas Y., Budak E., 1995, *Analytical Prediction of Stability Lobes in Milling*, Annals of the CIRP, Vol.44/1, pp.357-362.

[6] Altintas Y., Munasinghe W.K., 1996, *Modular CNC design for Intelligent Machining, Part 2: Modular Integration of Sensor based Milling Process Monitoring and Control Tasks*, Journal of Manufacturing Science and Engineering, Vol.118, pp.514-521.

[7] Altintas Y., Lee P., 1996, *A General Mechanics and Dynamics Model for Helical End Mills*, Annals of the CIRP, Vol.45(1), pp.59-64.

[8] Altintas Y., Engin S., Budak E., May 1999, *Analytical Stability Prediction and Design of Variable Pitch Cutters*, ASME Journal of Manufacturing Science and Engineering, Vol. 121, pp.173-178.

[9] Altintas Y., 2000, *Manufacturing Automation*, Cambridge University Press.

[10] Altintas Y., 2000, *Modelling Approaches and Software for Predicting the Performance of Milling Operations at MAL-UBC*, Machining Science and Technology, Vol.4(3), pp.445-478.

[11] Armarego E.J.A., Epp C.J., 1970, *An Investigation of Zero Helix Peripheral Up-Milling*, International Journal of Machine Tool Design and Research, Vol.10, pp.273-291.

[12] Armarego E.J.A., Wang J., Deshpande N.P., 1995, *Computer-Aided Predictive Cutting Model for Forces in Face Milling Allowing for Tooth Run-Out*, Annals of the CIRP, Vol.44 (1), pp.43-48.

[13] Armarego E.J.A., Deshpande N.P., 1993, *Force Prediction Models and CAD/CAM software for Helical Tooth Milling Processes. i. Basic Approach and Cutting Analyses*, International Journal of Production Research, Vol.31(8), pp.1991-2009.

[14] Bailey T., Elbestawi M.A., El-Wardany T.I., Fitzpatrick P., 2002, *Generic Simulation Approach for Multi-Axis Machining, Part 1: Modeling Methodology*, Transactions of the ASME, pp.624-633.

[15] Bailey T., Elbestawi M.A., El-Wardany T.I., Fitzpatrick P., 2002, *Generic Simulation Approach for Multi-Axis Machining, Part 2: Model Calibration and Feed Rate Scheduling*, Transactions of the ASME, pp.634-642.

[16] Budak E., 1994, *Mechanics and Dynamics of Milling Thin Walled Structures*, University of British Columbia, Ph.D. Thesis.

[17] Budak E. Altintas Y., 1994, *Peripheral Milling Conditions for Improved Dimensional Accuracy*, International Journal of Machine Tools and Manufacture, Vol.34(7), pp.907-918.

[18] Budak E., Altintas Y., Armarego E.J.A., 1996, *Prediction of Milling Force Coefficients From Orthogonal Cutting Data*, Transactions of the ASME, Vol.118, pp.216-224.

[19] Budak E., 2000, *Improving Productivity and Part Quality in Milling of Titanium Based Impellers by Chatter Suppression and Force Control*, Annals of the CIRP, Vol.49(1), pp.31-36.

[20] Clarke D.W., Mohtadi C., Tuffs P.S., 1987, *Generalized Predictive Control - Part I, The Basic Algorithm*, Automatica, Vol.23(2), pp.137-148.

[21] Engin S., Altintas Y., 1999, *Generalized Modeling of Milling - Mechanics and Dynamics: Part I: Helical End Mills*, ASME International Mechanical Engineering Congress and Exposition Symposium, Machining Science and Technology.

[22] Engin S., Altintas Y., 1999, *Generalized Modeling of Milling - Mechanics and Dynamics: Part II: Inserted Cutters*, ASME International Mechanical Engineering Congress and Exposition Symposium, Machining Science and Technology.

[23] Fussell B.K., Jerard R.B., Hemmett J.G., May 2001, *Robust Feedrate Selection for 3-Axis NC Machining Using Discrete Models*, Transactions of ASME, Vol. 123, pp.214-224.

[24] Fussell B.K., Jerard R.B., Richards N., Yalcin C., 2002, *NC Machining Feedrate Optimization Using On-Line Model Tuning and Adaptive Control*, Proceedings of the 2002 NSF Design and Manufacturing Research Conference.

[25] Huang X, 2003, *Internal Report at UBC MAL.*

[26] Jerard R.B., Fussell B.K, Hemmett J.G., Ercan M.T., 2000, *Toolpath Feedrate Optimization: A Case Study*, Proceedings of the 2000 NSF Design & Manufacturing Research Conference.

[27] Kang M., Lee S.-K., Ko S.-L., *Optimization of Cutting Conditions Using Enhanced Z Map Model*, Annals of the CIRP, Vol.51 (1), pp.429-432.

[28] Ko J.H., Yun W.-S., Cho D.-W., Ehmann K.H., 2002, *Development of a virtual machining system, part 1: approximation of the size effect for cutting force prediction*, International Journal of Machine Tools & Manufacture, Vol.42, pp.1595-1605.

[29] Koenigsberger F., Sabberwal A.J.P., 1961, *An Investigation into the Cutting Force Pulsations during Milling Operations*, International Journal of Machine Tool Design and Research, Vol 1, pp.15-33.

[30] Martellotti M.E., 1941, *An Analysis of the Milling Process*, Transactions of ASME, pp.677-700.

[31] Martellotti M.E., 1945, *An Analysis of the Milling Process Part II: Down Milling*, Transactions of ASME, Vol. 67, pp.233-251.

[32] Merrit H.E., 1965, *Theory of Self-Excited Machine-Tool Chatter*, Trans. ASME Journal of Engineering for Industry, Vol.87, pp.447-454.

[33] Richards N.D., Fussell B.K., Jerard R.B., 2002, *Efficient NC Machining Using Off-Line Optimized Feedrates and On-Line Adaptive Control*, Manufacturing Engineering Division: Symposium on Process Planning and Process Optimization, 2002 IMECE.

[34] Sabberwal A.J.P., 1961, *Chip Section and Cutting Force during the Milling Operation*, CIRP Annals, Vol.10, pp.197-203.

[35] Saturley P.V., Spence A.D., 2000, *Integration of Milling Process Simulation and On-Line Monitoring and Control*, International Journal of Advanced Manufacturing Technology, pp.92-98.

[36] Spence A.D., 1992, *Solid Modeller Based Milling Process Simulation,* University of British Columbia, Ph.D. Thesis.

[37] Spence A.D., Altintas Y., 1991, *CAD Assisted Adaptive Control for Milling*, Journal of Dynamic Systems, Measurement and Control, Transactions of the ASME, Vol.113, pp.444-450.

[38] Spence A.D., Altintas Y., Kirkpatrick D., 1990, *Direct Calculation of Machining Parameters from a Solid Model*, Journal of Computers in Industry, Vol.14., No.4, pp.271-280.

[39] ***Spence A.D., Li Z., XXXX, *Parallel Processing for 2-1/2 D Machining Simulation,*

[40] Suh S.-H., Cho J.-H., Hascoet J.-Y., 1996, *Incorporation of Tool Deflection in Tool Path Computation: Simulation and Analysis*, Journal of Manufacturing Systems, Vol.15, no.3, pp.190-199.

[41] Tlusty J., Polacek M., 1963, *The Stability of Machine Tools Against Self Excited Vibrations in Machining*, International Research in Production Engineering, ASME, pp. 465-474.

[42] Tlusty J., MacNeil P., 1975, *Dynamics of Cutting Forces in End Milling*, Annals of the CIRP, Vol.24, pp.21-25.

[43] Tobias, S.A., 1965, *Machine Tool Vibration*, Blackie.

[44] Tsai M.D., Takata. S. et al., 1990, *Prediction of Chatter Vibrations by Means of a Model-Based Cutting Simulation System*, Annals of the CIRP, Vol.39(1), pp.447-450.

[45] van Luttervelt C.A., Childs T.H.C., et al., 1998, *Present Situation and Future Trends in Modelling of Machining Operations*, CIRP STC Cutting Keynote Paper.

[46] Yellowley I., Kusiak A., 1985, *Observations on the Use of Computers in the Process Planning of Machined Components*, Transactions of the ASME, Vol.9(2), pp.70-74.

[47] Yun W.-S., Ko J.H., Cho D.-W., Ehmann K.H., 2002, *Development of a virtual machining system, part 2: prediction and analysis of a machined surface error*, International Journal of Machine Tools & Manufacture, Vol.42, pp.1607-1615.

[48] Yun W.-S., Ko J.H., Lee H.U., Cho D.-W., Ehmann K.H., 2002, *Development of a virtual machining system, part 3: cutting process simulation in transient cuts*, International Journal of Machine Tools & Manufacture, Vol.42, pp.1617-1626.